Multiproxy assessment of Holocene relative sea-level changes in the western Mediterranean: sea-level variability and improvements in the definition of the isostatic signal

Matteo Vacchi[1*], Nick Marriner[2], Christophe Morhange[1], Giorgio Spada[3], Alessandro Fontana[4], Alessio Rovere[5]

[1]Aix-Marseille Université, CEREGE CNRS-IRD UMR 34, Europole de l'Arbois BP 80, 13545 Aix-en-Provence, Cedex 4, France.

[2]CNRS, Chrono-Environnement UMR 6249, Université de Franche-Comté, UFR ST, 16 route de Gray, 25030 Besançon, France.

[3]Università degli Studi di Urbino, Via Santa Chiara 27, Urbino, Italy.

[4] Università degli Studi di Padova, Dipartimento di Geoscienze, Via Gradenigo 6, Padova, Italy.

[5]University of Bremen, Marum, ZMT, Bremen, Germany

[*]vacchi@cerege.fr

Abstract

A review of 914 Relative Sea-Level (RSL) data-points has resulted in the first quality-controlled database constraining the Holocene sea-level histories of the western Mediterranean Sea (Spain, France, Italy, Slovenia, Croatia, Malta and Tunisia). We reviewed and standardized the geological RSL data-points using a new multi-proxy methodology based on: (1) modern taxa assemblages in Mediterranean lagoons and marshes; (2) beachrock characteristics (cement fabric and chemistry, sedimentary structures); and (3) the modern distribution of Mediterranean fixed biological indicators. These RSL data-points were coupled with the large number of archaeological RSL indicators available for the western Mediterranean. We assessed the spatial variability of RSL histories for 22 regions and compared these with the ICE-5G VM2 GIA model. In the western Mediterranean, RSL rose continuously for the whole Holocene with a sudden slowdown at ~7.5

ka BP and a further deceleration during the last ~4.0 ka BP, after which time observed RSL changes are mainly related to variability in isostatic adjustment. The sole exception is southern Tunisia, where data show evidence of a mid-Holocene high-stand compatible with the isostatic impacts of the melting history of the remote Antarctic ice sheet.

Our results indicate that late-Holocene sea-level rise was significantly slower than the current one. First estimates of GIA contribution indicate that, at least in the northwestern sector, it accounts at least for the 25-30% of the ongoing sea-level rise recorded by Mediterranean tidal gauges. Such contribution is less constrained at lower latitudes due to the lower quality of the late Holocene index points. Future applications of spatio-temporal statistical techniques are required to better quantify the gradient of the isostatic contribution and to provide improved context for the assessment of 20th century acceleration of Mediterranean sea-level rise.

Keywords: Mediterranean Sea; Holocene; sea-level database; isostatic adjustment; sea-level proxy.

1. Introduction

Relative Sea-Level (RSL) changes since the Last Glacial Maximum (LGM, ~30 to ~20 ka BP) primarily document the transfer of ice mass from the continents to the oceans during deglaciation (e.g. Peltier and Fairbanks, 2006, Deschamps et al., 2012). Approximately 50 million km^3 of ice have melted from land-based ice sheets, raising RSL in regions distant from the major glaciation centers (far-field sites) by ~135 m (e.g. Bard et al., 1996; 2010; Lambeck and Purcell, 2005; Lambeck et al., 2014). During the Holocene (the last ~12 ka BP), empirical studies and Glacial Isostatic Adjustment (GIA) models show that the rate of ice-mass transfer decreased significantly at ~7 ka BP, when the Earth entered into a period of near RSL stability, after which time the ocean volume changed by just a few meters (e.g. Mitrovica and Milne, 2002; Lambeck et al., 2014).

On a regional scale, the interplay of glacio- and hydro- isostatic processes plays a significant role in defining the Holocene RSL changes. However, other factors have influenced RSL histories as well. Vertical tectonic displacements often appear to be continuous and gradual over time, but frequently consist of large

53 movements, for instance during earthquakes of great magnitude (e.g. Pirazzoli et al., 1994; Nelson et al.,
54 1996; Dura et al., 2014) or volcanic activity (e.g., Morhange et al., 2006). Local factors include
55 modifications of the tidal regime (e.g., Hall et al., 2013) and sediment consolidation due to the accumulation
56 of overlying material and land reclamation (e.g., Törnqvist et al., 2008; Marriner et al., 2012a).
57 Databases of RSL have been developed to better understand these forcing mechanisms of sea-level change,
58 to identify regional variations and to constrain geophysical models of glacial isostasy (e.g., Engelhart and
59 Horton, 2012; Shennan et al., 2012; Kahn et al., 2015).
60 For the Mediterranean, regional compilations of sea-level data have been produced for both the eastern and
61 the western Mediterranean (e.g., Lambeck and Bard, 2000; Vött, 2007; Lambeck et al., 2004a; Antonioli et
62 al., 2009; Vacchi et al., 2014). These studies used a variety of observational sea-level data from different
63 geomorphic settings and archaeological sites to produce RSL data-points. However, a standardized
64 methodology for the production of sea-level index and limiting points (crf. Gehrels and Long, 2007; Hijma et
65 al., 2015) is presently lacking for the Mediterranean region.
66 In this paper, we reconsidered and reanalysed the published sea-level data for the western Mediterranean
67 seaboard following the protocol described by the International Geoscience Programme (IGCP) projects 61,
68 200, 495 and 588 (e.g., Preuss, 1979; van de Plassche, 1982; Gehrels and Long, 2007; Shennan et al., 2015)
69 Here we present: i) a standardized methodology to produce sea-level index and limiting points from
70 published data deriving from the Mediterranean and ii) a comprehensive database of index and limiting
71 points from 14 ka BP to present, for 22 areas in the western Mediterranean (figure 1).
72 After summarizing the previous studies and reporting the unresolved issues regarding relative sea level in the
73 western Mediterranean (section 2), we outline the reasons for grouping sea-level data into 22 regions (section
74 2.2). We then explain our methodology to produce sea-level index and limiting points (section 3) and how
75 we predicted the RSL models using the open source numerical code SELEN (section 4). In section 5, we
76 reconstruct the RSL histories of the 22 regions using quality controlled sea-level index and limiting points.
77 We then discuss the applicability of our multiproxy approach in the Mediterranean (section 6.1), we compare
78 and contrast the reconstructed RSL histories with the predicted RSL models (section 6.2) and, finally, we
79 assess the spatial variability of late Holocene RSL changes in the western Mediterranean providing new
80 insights about the influence of the isostatic contribution on the current sea-level rising rates (6.3).

2. Study area

The study area encompasses the western Mediterranean coast at latitudes comprised between 45.7°N and 33°N and longitudes comprised between -0.3°E and 16.2°E (figure 1). The data were collected in central and northern Spain, southern France and Corsica, much of the Italian coast (including Sicily and Sardinia), Malta, Slovenia, northern and central Croatia and southern Tunisia (figure 1).

Western Mediterranean tides have an average amplitude of about 0.4 m, although they do show spatial variability based on coastal geometry and bathymetry (Tsimplis et al., 1995, Antonioli et al., 2015). Tidal amplitude is very small near the amphidromic points but it may reach amplitudes of up to 2 m in the Gulf of Gabes and the North Adriatic Sea (Tsimplis et al., 1995, Marcos et al., 2009). Around the Straits of Gibraltar, the Atlantic Ocean affects Mediterranean tides in the Alboran Sea (figure 1), but its influence rapidly declines further east (e.g., Marcos et al., 2009). Three main deltas, the Ebro, the Rhone, and the Po, represent the main sedimentary inputs into the western Mediterranean basin (Maselli and Trincardi, 2013; Anthony et al., 2014).

From a geological point of view, the western Mediterranean is a tectonically complex area where two small oceanic basins (the Tyrrhenian and Liguro-Provençal back-arc basins) occur along the Nubia-Eurasia convergent margin and are separated by the Corsica-Sardinia rigid continental block (figure 2, Jolivet and Faccenna, 2000; Jolivet et al., 2008; Faccenna et al., 2014).

In the western Mediterranean, some parts of the back-arc basin margins are undergoing compressional tectonics (e.g., Billi et al., 2011). This tectonic regime is particularly active, from west to east, along the east-Alboran, Algerian, and south-Tyrrhenian margins (Billi et al., 2011, Faccenna et al., 2014; figure 2). In the central Mediterranean, the contractional orogen swings around the Adriatic Sea and marks the deformed margins of Adria (figure 2).

2.1. Original source of the data

The post-LGM RSL changes in the western Mediterranean have been investigated since the late 1960s (e.g., Flemming, 1969; Pirazzoli, 1976; Lambeck and Bard, 2000; Lambeck et al., 2004a; Pirazzoli, 2005; Antonioli et al., 2009; Anzidei et al., 2015). In particular, several studies have focused on the late Holocene (last 4 ka) using geo-archaeological archives to reconstruct past sea-level histories in areas of Spain (e.g.,

109 Carmona-Gonzàles and Ballester, 2011), France (e.g., Morhange et al., 2001; 2013), Sardinia (e.g., Antonioli
110 et al., 2007; Orrù et al., 2011; 2014), Croatia (e.g., Antonioli et al., 2007; Faivre et al., 2010), Tunisia (e.g.,
111 Anzidei et al., 2011), Sicily (e.g., Scicchitano et al., 2008) and Malta (e.g., Marriner et al., 2012b; Furlani et
112 al., 2013). One of the main goals of the geoarchaeological studies has been to establish the RSL histories
113 during since the first millennium BC (e.g., Pirazzoli, 1976, Morhange et al., 2001, Lambeck et al., 2004b;
114 Goiran et al., 2009; Evelpidou et al., 2012). In Marseille's ancient harbour, Morhange et al., (2001), coupled
115 geo-archaeological and biological sea-level data to reconstruct RSL changes since the Bronze Age. They
116 proposed that RSL was at ~-1.5 m in the Middle Bronze Age (~3.6 ka BP) and ~-1.2 m in the Late Bronze
117 Age (~2.8 ka BP). Between the Archaic and Roman periods (~2.0 to 1.5 ka BP), RSL ranged between -0.8
118 and -0.7 m with respect to the current Mean Sea Level (MSL).
119 An ongoing debate concerns the archaeological interpretation of ancient Roman fish-tanks (*piscinae*), with
120 implications for the reconstruction of RSL during the Roman period. These coastal structures are assumed to
121 be amongst the most reliable archaeological RSL indicators (Lambeck et al., 2004b; Auriemma and Solinas,
122 2009; Morhange and Marriner, 2015) because sea level and fish-tank architecture are closely correlated and
123 their chronology is well constrained to between ~1st century BC (~2.1 ka BP) and ~1st century AD (~1.9 ka
124 BP).
125 Lambeck et al. (2004b) reported an extensive analysis of fish tanks in the Tyrrhenian Sea, and calculated
126 Roman RSL at ~-1.3 m MSL. The archaeological interpretation was based on both field surveys and on the
127 analysis of original Latin descriptions. Important features in the fish-tank architecture are: i) the sluice gate
128 (*cataracta*) that controlled water exchange between the tanks and the open sea, whilst not permitting the fish
129 to escape; ii) channels that assured water exchange, sometimes carved into the rocky bedrock; iii) foot-walks
130 (walking surfaces, *crepidines*) delimiting the fish tank basin and generally occurring at two or three levels
131 (Schmiedt, 1972).
132 Lambeck et al., (2004b) proposed that the upper limit of RSL in Roman times was 0.2 m below the lowest
133 walking surface (*crepido*). Lambeck et al. (2004b) and subsequently Auriemma and Solinas (2009)
134 suggested that the flow of water inside the fish tanks was tidally controlled by the palaeo mean lower water
135 denoted by the channel thresholds, often corresponding to the base of the mobile *cataracta*. Such an

136 archaeological interpretation has since been applied to a number of other coastal areas in the western
137 Mediterranean (e.g., Antonioli et al., 2007; 2011; Anzidei et al., 2011).
138 Evelpidou et al. (2012) also performed a detailed survey of the Tyrrhenian Sea's fish tanks proposing that
139 RSL in the Roman period ranged between ~-0.6 and ~-0.3 m MSL. These authors disagreed with the
140 interpretation of an original supratidal position for the lowest *crepido* stating that the height of the *cataracta*
141 proposed by Lambeck et al., (2004b) would not have been sufficient for the fish tanks to function properly.
142 Furthermore, Evelpidou et al., (2012) stated that the channel threshold and the base of the *cataracta* can be
143 located at any depth in the basin and, therefore, they cannot be considered a reliable sea-level indicator.
144 More recently, Morhange et al., (2013) used the palaeo-biological zoning of fixed marine fauna inside a
145 Roman fish tank at Frejus (France) to infer RSL at that time. They suggested that, at Frejus, the fixed gates
146 were built in subtidal position and were positioned at least 0.3 m below the upper limit of in situ fixed
147 marine organisms (*Serpulidae* spp, *Cladocora caespitosa* and *Ostrea* spp.).
148 In contrast to the late Holocene, there is comparatively less data for early to mid Holocene RSL changes in
149 the western Mediterranean. Lambeck and Bard, (2000), compiled a comprehensive assessment of RSL
150 variations in southern France for the last 30 ka BP. Similarly, Correggiari et al., (1996), Lambeck et al.,
151 (2004a; 2011) and Antonioli et al., (2009) assessed the postglacial RSL changes along the Italian peninsula
152 and Croatia. RSL history since the mid-Holocene has been investigated in France (e.g., Laborel et al., 1994;
153 Vella and Provencal, 2000), Tunisia (e.g., Jedoui et al, 1998; Morhange and Pirazzoli, 2005), Corsica and
154 Sardinia (e.g., Laborel et al., 1994; Antonioli et al., 2007). Significant sea-level data have also been collected
155 as part of coastal investigations with other purposes, for example, studies of Holocene environmental
156 changes in marshes and coastal lagoons in Spain (e.g., Dupré et al., 1988; Marco Barba et al., 2013), France
157 (e.g., Raynal et al., 2010; Sabatier et al., 2010), Sardinia (e.g., Di Rita and Melis, 2013; Orrù et al., 2014),
158 Tunisia (e.g., Lakhdar et al., 2006; Zaibi et al., 2011) as well as along the Adriatic (e.g., McClennen and
159 Housley, 2006; Caldara and Simone, 2005) and Tyrrhenian (e.g., Di Rita et al., 2010; Sacchi et al., 2014)
160 coasts of Italy.
161 We further used sea-level data provided by studies focused on neotectonics and palaeo-tsunami impacts in
162 Sicily (e.g., De Martini et al., 2010; Gerardi et al., 2011) and along the Adriatic coast (e.g., Furlani et al.,
163 2011; Marriner et al., 2014). Other coastal studies with sea-level data have focused on the sedimentary

164 evolution of large deltas (e.g., Somoza et al., 1995; Vella et al., 2005; Amorosi et al., 2008a) and other major
165 coastal plains (e.g., Dubar and Anthony, 1995; Rossi et al., 2011; Milli et al., 2013). Finally, we extracted
166 sea-level data from cores undertaken within the framework of the recently updated Italian Geological Maps
167 (e.g. Cibin and Stefani, 2009; Sarti et al., 2009).
168
169 *2.2. Database subdivision*
170 To account for the spatial variability of RSL changes we divided the database into 22 regions (figures 1 and
171 2) on the basis of (1) geographical position, (2) proximity to other RSL data-points (commonly a function of
172 local geomorphology, such as coastal plains between headlands, (Engelhart et al., 2015), and (3) the regional
173 neotectonic setting derived from the elevation of the last interglacial shoreline (MIS 5e, data from Ferranti et
174 al., 2006; 2010, Pedoja et al., 2014, if not otherwise specified, figure 2) and, secondarily, from the on-going
175 GPS-derived vertical velocities (data from Serpelloni et al., 2013, Figure 2).
176 Probabilistic assessment suggests that sea-level elevation during the last interglacial (~125 ka ago) was ~7.2
177 m above the present MSL (Kopp et al., 2009). In figure 2, the dark and pale green boxes (50 km^2 squares)
178 show the average elevation of the MIS 5e shoreline (as reported by Ferranti et al., 2006 and Pedoja et al.,
179 2014). Dark green boxes indicate average elevation of between 7.5 and 15 m (stable to very minor uplift)
180 while pale green indicates elevation between 0 and 7.5 m (stable to very minor subsidence). These regions
181 can be considered as being affected by a long-term vertical movement of between -0.06 and +0.06 mm a^{-1},
182 averaged for the last ~125 ka. It is worth highlighting that such vertical rates include both tectonics and the
183 GIA signal (Dutton and Lambeck, 2012), and that uplift/subsidence rates are probably not linear over the last
184 125 Ka.
185 In order to better understand the current vertical movements, we also analysed on-going vertical movements
186 recorded by GPS. Discrepancies between long-term vertical velocities and GPS measurements were
187 elucidated for some regions. Western Mediterranean GPS trends are based on short records (often less than
188 15 years, Serpelloni et al., 2013). Thus, they can give insights into the on-going vertical movements but are
189 less representative of the general vertical trend of a given region with respect to the MIS 5e elevation. For
190 this reason, we primarily used the long-term vertical velocities provided by the elevation of the last
191 interglacial shoreline for the subdivision of our database

192 We subdivided the Spanish Mediterranean coast into two regions (figures 1 and 2). Central Spain (#1)
193 extends between Alicante and the Gulf of Valencia and represents the westernmost region in our database. In
194 this area, historical seismicity is reported (Olivera et al., 1992). GPS vertical velocities document a general
195 subsidence trend with rates lower than 2 mm a^{-1} in this region, notably in the Gulf of Valencia. The northern
196 Spanish coast (#2) extends from the Ebro Delta to Cap Creus, at the border with France (figure 2). GPS-
197 derived vertical velocities indicate zero vertical motion in most of the regions, with the exception of the Ebro
198 and Llobregat deltas that show subsidence of 1.5 mm a^{-1}.
199 The central French coast extends from Cape d'Agde to Port Cros Island, including the Rhone Delta. GPS-
200 derived vertical velocities suggest zero ongoing vertical motion. The elevation of MIS 5e shorelines denotes
201 a long-term stability of the area (Ambert, 1999).
202 We subdivided the northern coast of the Ligurian Sea into two regions (figures 1 and 2). The western
203 Ligurian Sea (#4) encompasses the coastline between Frejus (France) and Genoa (Italy). Nonetheless,
204 although both MIS 5e and GPS-derived velocity fields indicate negligible vertical movement across the
205 whole area (figure 2), Dubar et al., (2008) documented a mild uplift (up to 0.06 mm a^{-1}) around the over-
206 thrusting Nice Range on the basis of the local MIS 5e elevation.
207 The eastern Ligurian sea region (#5) stretches from La Spezia to the Arno river coastal plain (figure 2). Both
208 GPS and long-term vertical velocities indicate a general subsidence trend of this region, with rates of up to
209 ~0.26 mm a^{-1} on the Versilia coastal plain.
210 Corsica and Sardinia show a general tectonic stability since the last interglacial (Ferranti et al., 2006; figure
211 2). They occupy the central sector of the western Mediterranean, and they were subdivided into the following
212 three regions, northern Corsica and Pianosa, (#6), southern Corsica-Northern Sardinia (#7) and southwestern
213 Sardinia (#8) according to the geographical distribution of the data. Sea-level data from Pianosa Island were
214 included in region (#6) due to its proximity to northern Corsica (figure 2). GPS-derived vertical velocities
215 indicate zero to weakly positive on-going vertical motion in the three regions (figure 2). The north-central
216 Latium region (#9) stretches from Civitavecchia to the Tiber Delta (figures 1, 2). In this region, GPS-derived
217 vertical velocities range from zero to less than 1 mm a^{-1} while stability to moderate uplift ($\leq$ 0.23 mm a^{-1}) is
218 documented since the last interglacial. On the Tiber Delta, long-term uplift of ~0.11 mm a^{-1} is reported.

219 The southern Italian coast presents a very complex tectonic setting (figure 2, Ferranti et al., 2010, Faccenna
220 et al., 2014). The Gulf of Gaeta region (#10) stretches from the Fondi to the Volturno coastal plains and
221 includes the Pontine Archipelago (figure 2). 0.3 to 0.2 mm a^{-1} of subsidence is reported on the Volturno plain
222 during the last ~40 ky BP. GPS-derived vertical velocities indicate a predominant on-going subsidence
223 across the area, with greater rates in the volcanic district of the Gulf of Naples (-8 mm a^{-1}, figure 2) where we
224 avoided the RSL reconstruction. In fact, it would be not indicative of the general RSL trend because this area
225 is strongly affected by significant non-eruptive crustal deformation (Morhange et al., 2006). Salerno Bay
226 (#11) includes the coastal plains of Sele River and is located south of the volcanic district of the Gulf of
227 Naples. The several MIS-5e shorelines found in the area indicate average long-term uplift ≤ 0.06 mm a^{-1} and
228 no nearby GPS-derived vertical velocities are available.
229 We have avoided RSL reconstructions from the tectonically-active Calabrian arc, (figure 2) which has been
230 affected by significant tectonic uplift since the last interglacial (Dumas et al., 2005; Ferranti et al., 2006;
231 2007). The highest rates of uplift are reported near Capo Vaticano (0.6 to 2 mm a^{-1} Tortorici et al. 2003;
232 Ferranti et al., 2010) and in the Messina Straits (~1.0-1.4 mm a^{-1}) between Calabria and Sicily (figure 2).
233 This uplift pattern is related to the interplay between regional and local (i.e. fault related) components of
234 vertical displacement (e.g., Ferranti et al., 2007; Scicchitano et al., 2011); rates of uplift decrease
235 progressively southwards and westwards of the Messina Strait (Ferranti et al., 2010). We have subdivided
236 the coasts of Sicily and Malta into three regions (figures 1, 2). The northwestern Sicily region (#12) stretches
237 from Palermo to Marsala, including Marettimo Island. The region shows on-going vertical movements ≤ 0.4
238 mm a^{-1} and is considered to have been tectonically stable since the last interglacial. The mid-eastern Sicily
239 region (#13) stretches from Catania to Syracuse. In this area, long-term uplift rates range between 0.4 and
240 0.7 mm a^{-1} (Dutton et al., 2009; Spampinato et al., 2011) and GPS data indicate on-going uplift ≤ 1 mm a^{-1}
241 decreasing southwards. In this area, large earthquakes and associated tsunamis have been recorded since
242 historical times (Scicchitano et al., 2007; De Martini et al., 2010).
243 Even if they are separated by about 100 km of sea, we grouped the southernmost part of Sicily and the
244 Maltese Islands into a single region (#14). These two sectors present zero to minimal on-going vertical
245 movement (figure 2) and very weak historical seismicity is reported for the area. The relatively shallow (≤ -

246 200 m) Malta Plateau presently divides these two coastal sectors, which were probably connected during the
247 LGM (Micaleff et al., 2012). Pedley (2011) reported the long-term tectonic stability of the Maltese Islands.
248 The southern Tunisia region (#15) represents the southernmost area of our database (figures 1 and 2). No
249 significant historical seismicity is reported in the region and several studies have underlined the tectonic
250 stability of southeastern Tunisia since the MIS 5e (figure 2, Jedoui et al., 1998).
251 We subdivided the northern Adriatic Sea into three regions (figure 1 and 2). The lagoons of Venice and
252 Friuli, (#16) stretch from the town of Venice to the town of Monfalcone including three large coastal lagoons
253 (Venice, Caorle and Grado-Marano); a long-term subsidence trend, ranging between 0.7 and 0.4 mm a^{-1}
254 (Carminati et al., 2003; Amorosi et al., 2008b), is reported in this region. GPS-derived data also indicate a
255 subsidence trend with rates higher than 2.5 mm a^{-1} (figure 2). The northeastern Adriatic region (#17)
256 encompasses the Gulf of Trieste (Italy and Slovenia) as well as the Istrian coast and the Island of Pag
257 (Croatia). On-going vertical movements are lower than -0.5 mm a^{-1} (figure 2), although there is no robust
258 information about the elevation of the MIS 5e coastline in this region. The area is affected by historical
259 seismicity up to M=6.0 in the southern sector (Herak et al., 1996).
260 The northwestern Adriatic region (#18) includes the southern part of the Po Delta and the whole Romagna
261 coastal plain. A major subsiding trend is documented across the area since the MIS 5e. High rates, up to 1
262 mm a^{-1}, occur near the Po Delta decreasing southwards to 0.6 mm a^{-1}. GPS-derived vertical motion also
263 indicates a clear pattern of subsidence, with rates higher than ~3 mm a^{-1} across the whole region.
264 We subdivided the central and southern Adriatic Sea into four regions. The mid-eastern Adriatic Sea (figures
265 1 and 2; #19) includes data from Vis and Bisevo Islands, located in the eastern part of the central Adriatic
266 Sea, in Croatia. Nearby GPS vertical velocities indicate zero motion. In this region, medium to strong
267 historical seismicity (such as the 1956 M=5.7 earthquake) is reported (Herak et al., 1996).
268 The mid-western Adriatic Sea (#20) includes data from the central coast of Abruzzo, between Pescara and
269 the Sangro coastal plain (figures 1 and 2). There is a paucity of long-term rates for vertical movements in this
270 region. Furthermore, GPS-derived vertical velocities are contrasting in this region (figure 2).
271 The northern Apulia region (#21) includes the eastern Gargano promontory and the Gulf of Manfredonia
272 (figures 1 and 2). To the west, the elevation of the MIS 5e shoreline on the Gargano promontory indicates
273 moderate uplift. Contrasting GPS-derived vertical velocities range from zero movement down to moderate

subsidence of ~0.5 mm a^{-1}. The region was historically affected by intense seismicity (Mastronuzzi and Sansò, 2002). As a consequence, the Holocene evolution of some sites on the western Gargano promontory (e.g., the Fortore River coastal plain and the Lesina Lake coastal barrier) have been strongly influenced by strong seismic events which produced co-seismic vertical displacements and devastating tsunamis (Mastronuzzi and Sansò, 2002; 2012). The southern Apulia region (figures 1, 2; #22) represents the easternmost areas of our database. Stability to weak subsidence since the last interglacial is reported for this region. This trend is corroborated by nearby GPS-derived vertical velocities.

3. Compilation of the Relative Sea-Level database

3.1 Indicators of former Relative Sea-Level

In order to produce an index point, the following information is required for each RSL indicator: (1) the location of the indicator; (2) the calibrated age of the indicator; and (3) the elevation of the indicator, corrected for the indicative meaning; (i.e. a known relationship between the indicator and a contemporaneous tidal level, the Mean Sea Level (MSL) in our database Shennan et al., 2015; Hijma et al., 2015). The indicative meaning is composed of a reference water level (RWL) and the indicative range (IR). The IR is the elevational range over which an indicator forms and the RWL is the midpoint of this range, expressed relative to the same datum as the elevation of the sampled indicator (e.g., Hijma et al., 2015, figure 3). Where a suite of quality controlled sea-level index points exist for a locality or region, they describe changes in RSL through time and can be used to estimate the rates of change. If a sea-level indicator did not show a clear and reasonably established relationship with the MSL, we converted it into a limiting point (see section 3.2). Although these data are not used to produce sea-level index points, they are extremely important in constraining the RSL above or below the terrestrial or limiting point (e.g., Shennan and Horton, 2002).

Tidal information was obtained from the National and International networks of tidal stations (e.g. IGN-Red de Maréografos, Spain; Service Hydrographique SHOM, France; ISPRA-Rete Mareografica Nazionale; HHI; Hrvatski Hidrografski Institut; Admiralty Tide Tables, UK). Local tidal measurements (e.g. Morhange and Pirazzoli, 2005) or tidal modelling (e.g. Antonioli et al., 2015) were also used.

In the following section we describe the different types of index points used in the database.

3.1.1. Fixed biological index points

Along the western Mediterranean coasts, the coralline rhodophyte *Lithophyllum byssoides* build reef-like bioconstructions just above MSL at the base of the mid-littoral zone (e.g., Péres and Picard, 1964; Laborel et al., 1994). Its lower limit is defined as the biological mean sea level (i.e. the sharp transition between the midlittoral and the infralittoral zone, Morri et al., 2004), which corresponds to the MSL with reasonable accuracy (≤ 0.1 m) in microtidal environments (e.g., Stiros and Pirazzoli, 2008; Schembri et al., 2005). *L. byssoides* rims are almost absent in very sheltered areas; they usually develop around the inlets of exposed coasts because the organic construction needs strong mixing of water but moderate wave impact to develop. Fossil rims of *L. byssoides* are accurate proxies for past RSL (e.g., Faivre et al., 2013; Rovere et al., 2015) and have been used for high-resolution (±0.1 to ±0.2 m of vertical uncertainty) RSL reconstructions in southern France and Croatia (e.g., Laborel et al., 1994, Faivre et al., 2013). *L. byssoides* has a very narrow vertical living range and rims form at and slightly above the biological mean sea level (i.e. in the upper midlittoral zone; Laborel and Laborel-Deguen, 1994; Laborel et al., 1994). The indicative range associated with these samples is from the Highest Astronomical Tide HAT to MSL (figure 3A, table 1). The database also includes four samples of fossil Vermetid reefs of *Dendropoma petraeum* collected in Sicily (region #12). The living range of these fixed Gastropoda is quite large (the lower intertidal to the infralittoral zones, Rovere et al., 2015). However, on the basis of the modern distribution of Vermetid reefs measured in Sicily (Antonioli et al., 1999; Lambeck et al., 2004a), we assigned an indicative range of MSL to Mean Lower Water MLW to these samples (figure 3A, table 1). This indicative range cannot be applied to other areas of the Mediterranean without a preliminary measurement of the local distribution of the living Vermetid reefs. Biological sea-level markers are not perfect horizontal lines but are naturally warped, even over short distances, due to local variations in hydrodynamics and morphology (Stiros and Pirazzoli, 2008; Faivre et al., 2013). For this reason, we added an environmental error of ±0.2 m to the fixed biological indicators included in the database.

3.1.2. Marsh and lagoonal index points

The majority of sea-level index points in previously published sea-level databases are salt-marsh deposits (e.g., Shennan and Horton, 2002; Engelhart and Horton, 2012). However, due to the microtidal regime of the

329 Mediterranean, salt-marsh areas are less developed than on oceanic coastlines and are usually concentrated
330 around large deltas (e.g., Somoza et al., 1998; Vella and Provensal, 2000) and downdrift coastal lagoons
331 (e.g., Silvestri et al., 2005; Marco-Barba et al., 2012).
332 For salt marshes, the indicative meaning was estimated using the present zonation of vegetation (e.g.,
333 Silvestri et al., 2005; Primavera et al., 2012) and microfossil assemblages (e.g., Serandrei-Barbero et al.,
334 2006; Caldara and Simone, 2005). The indicative range associated with samples of salt-marsh origin is from
335 the HAT to MSL (e.g., Hijma et al., 2015, figure 3B table 1). In the Rhone Delta, Vella and Provansal (2000)
336 found that the modern distribution of freshwater peats is between 0.1 and 0.6 m above the current MSL. This
337 indicative range was therefore applied to the samples from the Rhone and the Ebro deltas, which present a
338 similar geomorphic context (Somoza et al., 1998; Vella et al. 2005) and tidal range (Tsimplis et al., 1995).
339 The remaining freshwater peats of the database were conservatively transformed into terrestrial limiting
340 points (see section 3.2).
341 Coastal lagoons are a very common feature of Mediterranean coastlines. They are inland waterbodies,
342 usually developing parallel to the coast, typically separated from the open sea by a sandy barrier (e.g.,
343 Kjerfve, 1994; Anadòn et al., 2002). One or more restricted inlets ensure their continuous or intermittent
344 connection to the open sea. The water depth is generally less than 1 m and seldom exceeds a few meters
345 (e.g., McClennen and Housley, 2006; Marco-Barba et al., 2012; Sacchi et al., 2014).
346 Modern micro- and macro-fauna (e.g., Ruiz et al., 2005; Carboni et al., 2009; Nachite et al., 2010) and fossil
347 assemblages (e.g. Caldara et al., 2008; Amorosi et al., 2013; Marriner et al., 2012b) define two main types of
348 lagoonal facies in the Mediterranean.
349 (i) open or marine-influenced lagoon facies are generally characterized by sandy to silty sediments rich in
350 marine brackish molluscs such as *Cerastoderma glaucum* or *Bittium recticulatum*. This facies usually has
351 high species diversity (e.g., Marriner et al., 2012b). Foraminiferal and ostracods assemblages are dominated
352 by marine brackish or outer estuary taxa (e.g., *Aurila* spp., *Xestoleberis* spp., *Leptocythere* spp., *Loxoconcha*
353 spp.). Finding a direct relationship between these fossil assemblages and a palaeo MSL is challenging
354 because quantitative analysis of modern analogs are seldom reported in the literature. Nonetheless, we
355 produced index points using samples containing in situ *C. glaucum* mollusc shells, a euryhaline species
356 living in salinities of 4-100 ‰ and not tolerant of significant aerial exposure (Nikula and Väinölä, 2003;

357 Orrù et al., 2014). Since *C. glaucum* lives within the first 2 m of depth (Gravina et al., 1989; Lambeck et al.,
358 2004a; Primavera et al., 2012), we associated an indicative range from 0 to -2 MSL to the samples in outer or
359 marine-influenced lagoon facies (figure 3B, table 1).
360 ii) Inner or semi-enclosed lagoon facies show sedimentological and micropalaeontological features typical of
361 a brackish lagoonal/estuarine environments with lower species diversity with respect to the open marine
362 facies. There is a dominance of macrofossils typical of sheltered marine-lacustrine environments with the
363 presence of *Cerastoderma glaucum*, *Abra segmentum*, *Loripes lacteus* and *Hydrobiidae* spp. (e.g., Gravina et
364 al., 1989; Sabatier et al., 2010; Marriner et al., 2012b). Foraminifera, diatom and ostracod assemblages are
365 dominated by brackish inner estuarine species such as *Cyprideis torosa*, *Leptocythere lagunae*, *Loxoconcha*
366 *elliptica*, and *Cytherois fischeri*. The presence of opportunistic species tolerant of restricted conditions and
367 ample food availability, such as *Hyanesina germanica*, *Ammonia perlucida* and *Loxoconcha elliptica*, is
368 consistent with a low-energy, organic-rich lagoonal basin without significant oxygen depletion on the lagoon
369 bottom (Lachenal, 1989; Cimerman and Langer, 1991).
370 The evolution of a coastal lagoon from an open to semi-enclosed environment is commonly recorded in the
371 buried lagoonal successions of the Mediterranean's clastic coastlines, in a so-called regressive sequence
372 (e.g., Reineck and Singh, 1973; Caldara et al., 2008; Sabatier et al., 2010). The gradual development of
373 sandy barriers favours the progressive isolation of the brackish water body with consequent silting and
374 evaporation (Kjerfve, 1994). This leads to significant shallowing and silting of the semi-enclosed lagoons
375 with respect to the open lagoons. The depth of these lagoons seldom exceeds a few decimetres (e.g., Ruiz et
376 al., 2006; Vött, 2007) and the concomitant presence of macrophytes such as of *Ruppia maritima* and
377 *Lamprothamnium papulosum* is consistent with maximum lagoon depths of -1 m (e.g., Primavera et al.,
378 2011). Thus, samples found in inner or semi-enclosed lagoon facies (usually lagoonal shells, plant remains,
379 organic sediments, wood or charcoal) have an associated indicative range from 0 to -1 m (figure 3B, table 1).
380 We listed as undifferentiated brackish facies (figure 3B, table 1) those samples that did not provide enough
381 data to define a clear depositional environment (e.g., Correggiari et al., 1996) or that showed the presence of
382 marsh plant macrofossils together with micro- and macro-fossil assemblages ranging from
383 freshwater/slightly brackish taxa to shallow marine taxa (e.g., Colombaroli et al., 2007; Amorosi et al.,
384 2013). For these samples, we assumed an indicative range from HAT to Mean Lower Water MLW in order

385 to encompass the whole tidal zone (figure 3B, table 1). We added a further 0.5 m of additional error to
386 account for the environmental uncertainty.
387
388 3.1.3. Beachrock index points
389 Beachrocks are a lithified coastal deposit where lithification is a function of CO_3^{-2} ion concentration in
390 seawater, microbial activity and degassing of CO_2 from seaward flowing groundwater (Mauz et al., 2015b).
391 Field experiments and coastal observations (e.g., Hanor, 1978; Hopley, 1986; Neumeier, 1998) suggest that
392 cementation occurs within a few decades, in areas where suitable coastal morphology provides sufficient
393 accommodation space for soft sediment to settle (Mauz et al., 2015b). The cement by which the loose sand
394 and gravel are locked into position is indicative of the nearshore zone between the shoreface and the beach,
395 at the interface between seawater and meteoric water (e.g., Neumeier, 1998; Vousdoukas et al., 2007). Issues
396 on the use of beachrocks as accurate sea-level indicators are present in the literature (e.g., Kellettat, 2006).
397 However, recent studies have demonstrated that the cement is crucial for identifying the spatial relationship
398 between the coastline and the zone of beachrock formation (e.g., Vousdoukas et al., 2007; Mauz et al.,
399 2015b).
400 Thus, a definition of the indicative meaning depends largely on the preservation of the original cement and
401 its link with other sedimentary information (e.g., Mauz et al, 2015b). In the Mediterranean region,
402 beachrocks have been sampled and dated down to -45 m (e.g., De Muro and Orrù, 1998; Orrù et al., 2004).
403 Many studies have determined the vertical accuracy of beachrock samples through SEM, petrographic and
404 cathodoluminescence analyses of cements with a precision up to ±0.25 m in microtidal settings (e.g.,
405 Desruelles et al. 2009; Vacchi et al., 2012b). Such vertical accuracy cannot be obtained without accurate
406 description of the chemistry, crystal form and fabric of the cement. In the intertidal zone, the metastable
407 aragonite and High Magnesium Calcite (HMC) form as irregularly distributed needles, isopachous fibres or
408 rims and micritic cement (Neumeier, 1998; Desruelles et al., 2009). Samples having these characteristics
409 have an indicative range spanning HAT to MLW (figure 3C, table 1). However, 11 beachrock samples in our
410 database did not meet these requirements because the original source did not contain enough information.
411 The beachrock formation zone (i.e. the mixing zone, Vousdoukas et al., 2007) can exceed the intertidal zone
412 ranging from slightly subtidal to supratidal (spray zone). The amplitude of this zone depends on wave

exposure and the local geomorphological setting and is not symmetrical with respect to the MSL because it is greater in the supratidal zone (Mauz et al., 2015b). For these samples, we thus adopted a conservative indicative range of +2 m MSL to -1 m MSL (figure 3C, table 1). In our opinion, such approximation largely encompasses the mixing zone amplitude for the microtidal coasts of the Mediterranean.

3.2. Sea-level limiting points

Terrestrial limiting points usually form at an elevation above HAT, but can form in the intertidal zone due to rising groundwater tables (e.g., Engelhart and Horton, 2012). Therefore, a conservative lower limit of MSL has been employed in this analysis. In this database, terrestrial limiting points are typically samples deposited in freshwater marshes and swamps, alluvial plains, archaeological soils and on the subaerial part of beaches (table 1).

Marine limiting points are typically samples deposited in open marine or prodelta environments as well as lagoonal environments that do not meet the requirements to be classified as index points. Further, in situ marine benthos (e.g. *Lithophaga* sp, *Mesophyllum* sp.) living in the infralittoral zone and with no direct relationship to a former midlittoral zone was converted into marine limiting point (table 1).

Reconstructed RSL points must fall below terrestrial limiting points and above marine limiting points (example in figure 3B).

3.3. Archaeological index and limiting points

The long history of human occupation in the Western Mediterranean has left rich archaeological evidence along its coastlines, including, for instance, harbours, fish tanks, slipways and coastal quarries. Auriemma and Solinas (2009) furnished a synthesis of archaeological sea-level proxies. Many different archaeological structures that were originally emerged, or in contact with seawater, today lie below MSL and therefore attest to a relative change in the position of the sea surface and the structure. The "functional height" of an archaeological sea-level indicator corresponds to the elevation of a specific architectural part with respect to the MSL position at the time of its construction (e.g., Antonioli et al., 2007). Ancient port interface structures (e.g., quays and jetties), fishtanks and fishponds represent the most reliable sea-level indicators (e.g.,

Marriner and Morhange, 2007; Auriemma and Solinas, 2009; Morhange and Marriner, 2015) and have been used to produce index points in our database. In section 2.2, we described the differences in the interpretations of fishtanks and fishponds as sea-level index points. There is considerable morphological variability in these structures (Higginbotham, 1997) and the definition of a standardized indicative meaning for the western Mediterranean scale is particularly challenging. For this reason, in our database the indicative meaning assigned to a fishtank index point encompasses the different archaeological interpretations (maximum two, see section 2.2) provided by the original papers.

A variety of coastal archaeological structures, such as coastal quarries, tombs, breakwaters and coastal roads can provide insights to reconstruct the RSL in a given area (Auriemma and Solinas, 2009). However, due to the difficulties in establishing a relationship with a former MSL, we used these archaeological markers as terrestrial limiting points. Submerged structures, including harbour foundations and wrecks as well as the fine-grained sediments deposited inside the ancient ports (e.g., Marriner and Morhange, 2007), were used to produce marine limiting points.

3.4 Altitude of former sea-level

For each dated index point, RSL is estimated using the following equation:

$$RSL_i = A_i - RWL_i \quad [1]$$

(Shennan and Horton, 2002), where A_i is the altitude and RWL_i is the reference water level of sample i, both expressed relative to the same datum; MSL in our analysis.

The total vertical error is obtained by adding in quadratic individual errors according to:

$$e_i = (e^2_1 + e^2_2 + e^2_3 + e^2_n \ldots)^{1/2} \quad [2]$$

(Shennan and Horton, 2002), where e_1, … e_n represent the sources of error for each index point i including the indicative range (figure 3). The additional errors comprise an error associated with calculating the sample

467 altitude. This can be as small as ±0.05 m with high precision surveying (e.g., Shennan, 1986), but can
468 increase to more than ±0.5 m when the altitude was estimated using the environment in which the sample
469 was collected (e.g., saltmarsh; Engelhart and Horton, 2012) or when the depths of the samples are measured
470 with diving gauges (e.g., Rovere et al., 2010; Vacchi et al., 2012a). In southern France and Corsica, many
471 data are expressed in relation to the local National Geodetic Datum (NGD) that is presently 0.1 m below
472 MSL (e.g. Vella and Provansal, 2000; Morhange et al., 2013). All the data levelled to the NGD were
473 therefore corrected.
474 A tidal error was included if the tidal information was based on multiple tidal stations. In our database this
475 error does not exceed ±0.1 m, due to the microtidal setting of the Mediterranean. We included a core
476 stretching/shortening sampling error ranging from ±0.15 m for rotary corers and vibracorers to ±0.05 m for
477 hand coring (Hijma et al., 2015). The sample thickness is also incorporated into the sampling error term. For
478 older bulk sediment samples, this may be as large as 0.25 m (e.g., Engelhart et al., 2015). We also calculated
479 the angle of borehole error as a function of the overburden of the sample, taken in this study to be 1 %
480 (Tornqvist et al., 2008). We also included an environmental error that can be as up to 0.5 m in saltmarsh and
481 lagoonal sediments not showing a clear depositional environment (see section 3.1.2.). The vertical error of
482 the archaeological index points is not constant and is strongly related to the archaeological interpretations
483 provided in the original papers. However, preservation of fossil biological zones on the archaeological
484 structures may provide vertical uncertainties of up to 0.05 m (Marriner and Morhange, 2015).
485 Because of the lack of specific Mediterranean studies, we decided to not include an error term for potential
486 changes in the palaeotidal range (e.g., Hill et al., 2011). Nonetheless, it cannot be excluded that this error
487 may have affected the indicative range of the data points during the Holocene.
488 To account for sediment compaction (e.g., Edwards, 2006), we subdivided the saltmarsh and lagoonal index
489 points into basal and intercalated categories (Horton and Shennan, 2009). Basal samples are those recovered
490 from within the sedimentary unit that overlies the incompressible substrate, but not directly at the
491 intersection between the two (e.g., Engelhart and Horton, 2012). Basal samples may have undergone some
492 consolidation since deposition. Intercalated samples correspond to organic horizons in between clastic layers
493 and, therefore, they are generally most prone to compaction (e.g., Hijma et al., 2015). Where stratigraphic

494 information was unavailable for an index point, we conservatively interpreted it as intercalated. Index points
495 from archaeological markers, fixed biological and beachrock samples are virtually compaction free.

496 ## 3.5 Age of sea-level indicators

497 In our database, the age of the samples was estimated using radiocarbon (^{14}C) dating of organic material
498 from salt and fresh water marshes, marine and lagoonal shells, beachrock bulk cement as well as from the
499 archaeological age of coastal structures. Because the production of atmospheric radiocarbon has varied
500 through geological time, radiocarbon ages were calibrated into sidereal years with a 2σ range. All samples
501 were calibrated using CALIB 7.0. We employed the IntCal13 and Marine13 (Reimer et al., 2013) datasets
502 for terrestrial samples and marine samples, respectively. Where available, information on the necessary
503 reservoir correction was taken either from the Marine Reservoir Database (Reimer and Reimer, 2001) or
504 from published values. All index points are presented as calibrated years before present (ka BP), where year
505 0 is AD 1950 (Stuiver and Polach, 1977). A concern with old radiocarbon ages is the correction for isotopic
506 fractionation (Tornqvist et al., 2015). This became a standard procedure at most laboratories by the late
507 1970s (Stuiver and Polach, 1977), but some laboratories have only applied this correction since the mid-
508 1980s (Hijma et al. 2015).

509 In the database, the majority of ages were analysed after 1990 and, therefore, most are not subject to this
510 potential error. For the 31 ages that are affected, we followed the procedure of Hijma et al. (2015) to correct
511 for isotopic fractionation. The age of the archaeological RSL data-points is given both by the period of
512 construction and/or by the ^{14}C dating of biological indicators fixed on the coastal structures (Morhange and
513 Marriner, 2015). In our database, the age of the archaeological RSL data-points is restricted to the last 5.0 ka
514 BP.

515

516 ### *3.6 Example of the production of a lagoonal index point from Malta*

517 In order to better explain our new methodology for the production of index points in the Mediterranean, we
518 here provide an example from a marsh coring in Malta. The sedimentary sequence from the coastal plain of
519 Burmarrad is presented in figure 4 (Marriner et al., 2012b). The core BM1 (35.93 N°; 14.41° E) was
520 obtained using a percussion corer (±0.15 m of sampling error) and has a surface elevation of +2 m MSL

obtained using a high accuracy GPS (±0.05 m of levelling error) and extends to -15 m MSL. The base of the core (-15 m to -11 m) is composed of a dark grey unit dominated by silts and clay (47-98%). A charcoal (±0.05 m of thickness error) was sampled 12.1 m below the surface (0.12 m of angle error) and -10.1 below MSL. Radiocarbon dating of the charcoal yielded 6500 ±30 ^{14}C years. The mollusc faunal density is low and dominated by lagoonal taxa (*Cerastoderma glaucum*, *Abra segmentum*) and the upper muddy-sand assemblage in sheltered areas (*Cerithium vulgatum*). The ostracods are dominated by brackish water (*Cyprideis torosa*) and freshwater (*Candona* cf. *lactea*, *Candona* cf. *compressa*, *Potamocypris variegata*, *Darwinula stevesoni*, *Illyocypris gibba*) species. The lagoonal taxa and low faunal densities indicate that the charcoal was deposited in an inner or semi-enclosed lagoon. Thus we assigned the charcoal sample a reference water at the midpoint between 0 and -1 m MSL (-0.5 m MSL) and an indicative range of 0 to -1 (± 0.5 m). We are aware that charcoal found in lagoons may have been transported and yield ages older than the lagoon. Nonetheless, this error is inferior to the error margins associated with radiocarbon dating. In this instance, multiple samples (charcoal and peats) yielded coherent ^{14}C ages for this unit (Marriner et al., 2012b) supporting the chronology for this lagoonal environment.

The calculation of RSL and age, including the error terms, for this index point was:

RSL = -9.1 m – (-0.5 m)

= -9.6 m

Error = Σ (0.5 $m^2_{\text{indicative range}}$ + 0.05 $m^2_{\text{levelling error}}$ + 0.2 $m^2_{\text{sampling and thikness errors}}$ + 0.12 $m^2_{\text{angle error}}$)$^{1/2}$ = 0.55 m

Age =6500 ±30 ^{14}C years

= (7326 ka 7471 ka BP 2σ).

4. Predictions of RSL

The RSL model predictions presented in the following sections have been obtained by solving the Sea-level Equation (SLE, Farrell and Clark, 1976). The SLE, which describes the spatiotemporal variations of sea-level associated with the melting of late Pleistocene ice sheets, has been solved numerically by means of an improved version of the open source code SELEN (Spada and Stocchi, 2007). SELEN assumes a laterally

548 homogeneous, spherical, incompressible and self-gravitating Earth with Maxwell rheology. It includes the
549 effects of rotational fluctuations on sea-level (Milne and Mitrovica, 1998) and accounts for horizontal
550 migration of shorelines following the method outlined by Peltier (2004). In all our computations, we have
551 employed the ICE-5G model of Peltier (2004) to predict a nominal RSL curve, based on a three-layer
552 approximation of the multi-layered viscosity profile VM2 (table 2). To account for the uncertainties in the
553 viscosity profiles, we performed further runs varying the viscosity profiles in each layer within a reasonable
554 range; the minimum and maximum viscosity values are shown in table 2. The thickness of the elastic
555 lithosphere has been kept constant (90 km) in all of our calculations.

556 5. Results

557 We re-assessed 914 radiocarbon and archeologically dated RSL data-points along the western Mediterranean
558 Sea. We reconstructed the RSL histories of 22 regions using a database composed of 469 index points and
559 175 limiting samples (appendix A, references of the original sources in appendix B, figure 5A,B). We
560 excluded 270 sea-level datapoints (122 index points and 158 limiting points), which were deemed to not be
561 appropriate for the RSL reconstructions (appendix C). For instance, we discarded the RSL data-points that
562 may have been significantly affected by local co-seismic tectonic uplift or subsidence. For example, near
563 Punta delle Pietre Nere (North Apulia region, #21), Mastronuzzi and Sansò (2002; 2012) provided evidence
564 for a co-seismic RSL change greater than 0.5 m at ~1624 AD. Similarly, on Pag Island (Nortwestern Adriatic
565 #17), detailed investigation indicated a co-seismic subsidence at ~1100 AD (Marriner et al., 2014).
566 Therefore, at sites where co-seismic vertical movements were documented by previous studies, we did not
567 use the RSL data-points older than the seismic event, whose current position was significantly influenced by
568 the rapid vertical movement. Obviously, we cannot exclude that presently unknown seismic events may have
569 influenced the position of some index points in tectonically active regions included in our database.
570 We further excluded the RSL data-points showing a high degree of compaction. For instance, an index point
571 placing the RSL at ~-11.1 m MSL at ~6.7 ka BP in the Rhone Delta (Southern France, #3, Vella et al., 2005,
572 appendix C) is inconsistent with a suite of points placing the RSL at least ~5 m higher at the same time. This
573 evaluation was only possible at sites where RSL reconstruction was based on multiple proxies.

574 Reconstructions based on small datasets or only on intercalated samples are thus less reliable and caution
575 must be used when comparing these data with the GIA models.
576 In addition, we rejected a large amount of data not useful for RSL reconstruction. For example, a marine
577 limiting point constraining the RSL above ~-14.2 m MSL at ~5.2 BP in Northern Corsica and Pianosa (#6,
578 Sartoretto et al., 1996, appendix C) is not useful because several other data-points demonstrate that RSL was
579 already above ~-6 m MSL at this time (figure 7, #6). Finally, we excluded samples with poor or absent
580 descriptions of the depositional environments.
581 Spatially, RSL reconstructions covered most of the north-western Mediterranean coast whereas Tunisia
582 represents the sole region located on the southern Mediterranean seaboard, where data paucity did not allow
583 a robust RSL reconstruction for Algeria and Morocco (figure 1). The age range of the data spans the last 14
584 ka, with constant increase in the number of index and limiting points throughout the Holocene (figure 5B).
585 Compaction-free index points (e.g., L. byssoides, beachrocks and archaeological index points) and basal
586 index points represent 28% and 14% of the database, respectively. The majority (52%) of the index points
587 included in the database is intercalated (figure 5B).

588 ## 5.1 Central Spain (#1)

589 The RSL history of the Central Spanish coast is composed of 13 index points and 13 limiting points (figure
590 6, #1) from coastal areas between Valencia and Alicante. The oldest index point places the RSL at -16.0 ±
591 0.6 m at ~9.1 ka BP. RSL rose to -10.6 ± 0.6 m at ~8.6 ka BP and to -6.1 ± 0,7 m at ~8.3 ka BP. Two points
592 document the progressive rise between ~8.3 and ~7.1 ka BP when an index point places the RSL at -3.5 ±
593 0.5 m. Two marine limiting points (shallow shoreface) indicate RSL was slightly above -2 m at ~6.5 ka BP.
594 Between ~6.0 and ~5.0 ka BP terrestrial samples constrain the RSL below the present datum. Late Holocene
595 intercalated index points show scatter, most likely related to sediment compaction. Less compacted index
596 points indicate that RSL was at -0.9 ± 0.6 m at ~3.4 ka BP and at -0.3 ± 0.5 m at 1.1 ka BP.

597 ## 5.2 Northern Spain (#2)

598 The Northern Spanish coast database is composed of 19 index points and 6 limiting points (figure 6, #2).
599 Index points and limiting dates derive from cores on the Ebro and Llobregat deltas and Cubelles coastal
600 plain, in addition to beachrocks and L. byssoides samples collected in Costa Brava. Archaeological

601 investigations near Empuriès provided marine limiting samples. At ~12 ka BP, RSL was at -40 ± 0.9 m.
602 Younger index points document that RSL rose rapidly to -12.1 ± 0.7 m at ~8.3 ka BP. The suite of mid
603 Holocene index points from Cubelles coastal plain indicates RSL was at -3.4 ± 0.8 m at ~5.7 ka BP and at -
604 1.2 ± 1.2 m at ~4.0 ka BP. Intercalated index points from the Ebro Delta show evidence of compaction, most
605 likely due to the weight of the overlying sediment body. In fact, at ~5.9 ka BP, one index point from the Ebro
606 Delta places the RSL at -9.1 ± 0.7 m and at ~3.6 ka BP at -6.6 ± 0.7 m. One L. byssoides index point
607 indicates RSL was already at -0.4 ± 0.5 m at ~2.3 ka BP. Thereafter, RSL remained within -0.7 m of present
608 day.

609 ## 5.3 Central France (#3)

610 The RSL history of central France is based on 80 index points and 16 limiting points (figure 6, #3). Data
611 derive from marsh and lagoon cores on the Rhone Delta, Berre lagoon and the Languedoc coastal area.
612 Samples comprise *L. byssoides* collected at Port Cros National Park and La Ciotat, as well as fixed fauna
613 from archaeological excavations in Marseille. One basal index point places the RSL at -43.3 ± 1.5 m at ~11.7
614 ka BP. Index and limiting points constrain a rapid sea-level rise to the early Holocene. At ~10.6 and at 7.5 ka
615 BP, RSL was at -29.9 ± 0.4 m and at -7.4 ± 0.4 m, respectively. The rate of RSL declined in the mid
616 Holocene. At 5.0 ka BP, multiple basal index points indicate RSL was ~-2.8 m. Index points for the last 4.6
617 ka BP show significant scatter. Basal peat samples from the Rhone Delta indicate a sea-level stillstand at ~-
618 2.5 m between ~4.6 and ~3.5 ka BP. Conversely, in the same period, both archaeological index points and L.
619 byssoides index points indicate a continuous rise in sea-level with multiple index points that constrain the
620 RSL to ~-1.5 m at ~3.5 ka BP. Rising rates decreased during the remaining part of the Holocene. Multiple
621 archaeological and *L. byssoides* index points indicate RSL was at ~-0.8 m at ~2.5 ka BP, rising to ~-0.8 m at
622 ~1.5 ka BP. During the last 1.0 ka BP, RSL remained within 0.3 m of modern MSL.

623 ## 5.4 Western Ligurian Sea (#4)

624 The RSL database of the western Ligurian Sea consists of 19 index points and 18 limiting dates (figure 7,
625 #4). Archaeological excavations in the ancient harbours near Frejus and Genova provided index and limiting
626 points. Additional data derived from cores performed on the coastal plains near Nice (France), Savona and
627 Genova (Italy). Index points also derived from *Lithophyllum byssoides* samples collected near Frejus and

628 Nice, and from a beachrock sample collected near Savona (Italy). At ~13.0 ka, index and limiting points
629 constrain the RSL to -45.6 ± 1.2 m. Then, RSL rose rapidly to -18 ± 0.9 m at ~9.3 ka BP. During the mid-
630 Holocene (from ~7.5 to ~5.7 ka BP), RSL was between -6.1 ± 1 m and -1.1 ± 1.1 m. Index points in the Late
631 Holocene show scatter. Archaeological and *L. byssoides* index points suggest a continuous rise of RSL, from
632 -0.9 ± 0.4 m at ~3.0 ka BP to -0.4 ± 0.3 at ~2.0 ka BP, followed by a gradual rise to the present datum.

633 ### 5.5 Eastern Ligurian Sea (#5)

634 The RSL history of the northeastern Ligurian Sea is based on 21 index points and 9 limiting points from
635 cores on the Versilia plain and the Arno river coastal plain (figure 7, #5). Additional data-points derive from
636 archaeological investigations near Pisa and La Spezia. RSL was at -45.1 ± 1.1 m at ~12.5 ka BP. Then, basal
637 index points indicate that RSL rose rapidly to -13.9 ± 1.0 m at ~8.0 ka BP and to -6.7 ± 0.6 m at ~6.6 ka BP.
638 RSL rise slowed down in the remaining part of the Holocene. At ~4.2 ka BP, multiple intercalated index
639 points place the RSL at ~-2.2 m. Late Holocene RSL is loosely constrained by the data. The youngest
640 intercalated index point places the RSL at -1 ± 0.6 m at ~2.2 ka BP. Younger terrestrial limiting points
641 constrain the RSL above -0.2 m at ~2.0 ka BP

642 ### 5.6 Northern Corsica and Pianosa (#6)

643 The RSL history for this region is restricted to the late Holocene and is presented in figure 7 (#6). The
644 database is composed of 15 index points from L. byssoides samples collected in Scandola, and Cap Corse in
645 northern Corsica. Additional index and limiting points derive from archaeological surveys carried out on
646 Pianosa Island (Italy). The oldest index point places the RSL at -1.5 ± 0.4 m at ~4.0 ka BP. Younger index
647 points show a continuous sea-level rise. RSL was at -0.8 ± 0.4 m at ~2.0 ka BP, at -0.5 ± 0.4 m at ~1.6 ka BP
648 and at -0.3 ± 0.4 m at ~1.0 ka BP. Archaeological index points place the RSL at -1.1 ± 0.2 m at ~2.0 ka BP
649 and at -0.8 ± 0.2 m at ~1.0 ka BP.

650 ### 5.7 Southern Corsica and northern Sardinia (#7)

651 The database for southern Corsica and northern Sardinia consists of 11 index points from beachrock samples
652 collected in the Bonifacio strait and in northeastern Sardinia (figure 7, #7). Additional limiting points were
653 obtained from cores in Gulf of Valinco (Corsica) and from archaeological surveys in Bonifacio Strait, Capo

Caccia, and Olbia (Sardinia). During the early Holocene, RSL rose from -33.5 ± 1.6 m at ~10.0 ka BP to -17.5 ± 1.6 m at ~8.3 ka BP. RSL is loosely constrained between ~8.0 and ~2.5 ka BP. Younger index and limiting points indicate RSL was between ~-0.7 and ~-1.5 m between ~2.0 and ~2.0 ka BP. At ~0.8 ka BP, one beachrock index point places the RSL at -0.8 ± 1.5 m.

5.8 Southwestern Sardinia (#8)

The RSL history of southern Sardinia comprises 18 index points and 8 limiting points (figure 8, #8). Data were obtained from cores in Cagliari, in the Gulf of Oristano, in Piscinni Bay and near archaeological sites in Tharros, Nora, Malfatano Cape and Sant'Antioco. The oldest index point at ~10.8 ka BP estimates that RSL was at -45.5 ± 1.6 m. RSL rose to -29.5 ± 1.0 m at ~9.7 ka BP and to -27 ± 1.0 m at ~9.4 ka BP. At ~7.0, RSL was at -13.9 ± 1 m MSL. Between ~4.6 and 4.0 ka BP, index points show considerable scatter. One intercalated sample from Cagliari places the RSL at -6.8 ± 1.0 m while one sample from Is Mistras places the RSL at -2.2 ± 1.0 m. Late Holocene index and limiting points indicate that RSL rose to within ~1.4 m of modern MSL from ~2.5 ka BP to present.

5.9 North-central Latium (#9)

The RSL history for the northern Latium coast spans the early Holocene to present and constitutes 36 index points and 13 limiting points (figure 8, #9). Data derive from salt and freshwater marshes from the Tiber Delta and from archaeological investigations carried out on the Tiber Delta (Portus and ancient Ostia), near Santa Marinella and Civitavecchia (figure 8, #9). The two oldest index points place the RSL at -43.9 ± 0.7 m at ~12.8 ka BP. A suite of intercalated and basal index points shows a rapid rise between ~12.7 and ~10.9 ka BP when RSL was at -28 ± 0.5 m. There is considerable scatter in the younger intercalated index points, probably reflecting the influence of water and organic content, long-term tectonic uplift and the depositional history of the Tiber Delta. At ~8.5 ka BP, multiple intercalated index points place the RSL at -8.9 ± 1.2 m and between -3.1 and -2.1 m at ~5.5 ka BP. The Late Holocene RSL history is poorly constrained.

At ~2.0 ka BP, different archaeological interpretations (see section 2.2) of Roman fishtanks place the RSL between ~-1.3 m and ~-0.4. At ~2. ka BP, one intercalated index point places the RSL at -0.6 ± 0.6 m and a further archaeological index point indicates RSL was at -0.8 ± 0.2 m at ~1.7 ka BP.

5.10 Gulf of Gaeta (#10)

The database for the northern Campania coast consists of 11 index points and 5 limiting points from cores on the Volturno and Fondi plain and archaeological surveys in Formia and the Pontine archipelago (figure 8, #10). A terrestrial limiting point suggests RSL was below ~-27.0 m at ~11.7 ka BP. The oldest intercalated index point places the RSL at -24.6 ± 1.0 m at ~8.8 ka BP. RSL rose to -7.5 ± 0.6 m at ~7.5 ka BP. At ~4.7 ka BP, one basal index point places the RSL at -4.1 ± 1.0 m. During the Late Holocene, one intercalated index point indicates RSL was at -2.6 ± 1.0 m at ~3.3 ka BP and at -1.0 ± 0.5 m at ~2.1 ka BP. During the same period, different archaeological interpretations of Roman fish tanks place the RSL between ~-1.3 and ~-0.6 ± 0.2 m.

5.11 Salerno Bay (#11)

The RSL history of Salerno Bay consists of 6 index points and 5 limiting points and is restricted to the mid-Holocene (figure 8, #11). Data are all from cores taken on the coastal plain of Sele river. Further limiting points derive from offshore coring in Salerno Bay. At ~9.3 ka BP, RSL was at -16.3± 1.1 m. RSL rose to -8.3 ± 1.1 m at ~8.4 ka BP. From ~8 to ~7.2 ka BP, limiting points constrain the RSL between -5.3 and -7.2 m. A younger index point places the RSL at -0.5 ± 1.0 m at ~4.1 ka BP.

5.12 Northwestern Sicily (#12)

The RSL history of northwestern Sicily comprises 9 index points and 5 limiting points. Data come from a lagoon core near Marsala and from fossil vermetid reefs in Capo San Vito and near Palermo (figure 9, #12). Additional limiting points derive from fossil marine shells collected on Marettimo Island and near Palermo and archaeological investigations in the Punic town of Mozia. The oldest limiting points constrain the RSL below ~-27 m and above ~-25 m at ~9.5 ka BP. There is a hiatus of data up to ~2.8 ka BP when an index point places the RSL at -1.1 ± 0.6 m. RSL rose to -0.4 ± 0.6 m at ~2.5 BP and was within ~0.3 m during the last 1 ka BP.

5.13 Mid-eastern Sicily (#13)

The database for mid-eastern Sicily includes 14 index points and 7 limiting points. Data are from archaeological surveys near Syracuse and lagoon cores near Augusta, Catania and Syracuse (figure 9, #13).

706 The oldest intercalated index point places RSL at -36.9 ± 1.1 m at ~9.6 ka BP. A limiting point constrains the
707 RSL above ~-20 m at ~8.1 ka BP. RSL rose rapidly to -6.2 ± 1.0 m at ~6.6 ka BP and to -2.3 ± 1.0 m at ~4.2
708 ka BP. Late Holocene data-points show significant scatter, most likely related to the uplift trend affecting the
709 area (see section 2.1). Intercalated index points from Augusta and Priolo indicate that RSL reached the
710 present datum at ~3.7 ka BP. Conversely, archaeological data-points indicate RSL was between -3 and -1.2
711 m at ~3.7 ka BP and at -1.5 m ± 0.3 m at ~2.6 ka BP.

712 ## 5.14 Southern Sicily and Malta (#14)

713 The RSL history for Southern Sicily and Malta is restricted to the mid and late Holocene. The database is
714 composed of 14 index points and 9 limiting points from lagoon cores near Pachino (Sicily) and in Burmarrad
715 (Malta). Additional limiting points derive from archaeological surveys undertaken in Avola (Sicily) and
716 along the Maltese coast near Marsaxlokk (figure 9, #14). The oldest intercalated index point places the RSL
717 at -11.1 ± 1.0 m at ~7.5 ka BP. At ~6.1 ka BP, index and limiting points constrain the RSL to ~-7 m. Two
718 index points indicate RSL was between -4.4 m and -3.2 m at ~4.7 ka. RSL slowed in the late Holocene. RSL
719 was at -2.1 ± 1.1 m at ~3.9 ka BP and at -1.8 ± 1.1 m at 2.8 ka BP. A limiting point constrains the RSL
720 below -0.8 m at ~2.0 ka BP. Multiple index and limiting points indicate RSL rose to within ~1 m of modern
721 MSL from ~1.5 ka BP to present.

722 ## 5.15 Southern Tunisia (#15)

723 The RSL database for the southern Tunisian coast includes 18 index points and 20 limiting points and is
724 restricted to the last ~7.4 ka BP (figure 9, #15). Data come from a lagoon core in the Gulf of Gabes, as well
725 as from beachrock samples and archaeological surveys undertaken near Djerba Island. RSL was –0.6 ± 0.9 m
726 at ~7.4 ka BP and rose to 0.1 ± 1.1 m at ~6.8 ka BP. Multiple index limiting points indicate RSL was above
727 the present MSL for the remaining part of the mid-Holocene. Two marine limiting points constrain it to
728 above 1.7 ± 0.3 m at ~5.5 ka BP while terrestrial limiting points suggest RSL did not exceed 1.4 ± 0.4 m
729 during the same period. At ~4.0 ka BP, RSL dropped to the present datum and remained within ~-0.4 m and
730 ~0.4 m in the late Holocene. Intercalated index points indicate RSL was at 0 ± 0.6 m at ~3.1 ka BP and at 0.1
731 ± 0.6 m at ~2.5 ka BP. At ~1.8 ka BP, two archaeological index points place the RSL at ~-0.3 m while an
732 intercalated index point places the RSL at 0.4 ± 0.6 m. At ~0.6 ka BP, RSL was at -0.1 ± 0.6 m.

5.16 Venice and Friuli lagoons (#16)

The RSL history in this region is composed of 49 index points and 8 limiting points (figure 10, #16). Most of the data are from coring and geoarchaeological surveys of Venice lagoon. Additional index and limiting points derive from cores on the Friuli coastal plain and the lagoons of Grado-Marano and Caorle, and near the town of Monfalcone. RSL is not well constrained in the early Holocene with the oldest limiting point placing the RSL below -23.5 m at ~9.7 ka BP. A suite of basal index points documents a continuous rise in RSL during the mid-Holocene. RSL was at -8.8 ± 0.6 m at ~7.5 ka BP rising to -5.5 ± 0.8 m at ~6.6 ka BP. At ~5.5 ka BP, index and limiting points indicate RSL was between -3 and -3.6 m. There is considerable scatter in the late-Holocene index points, most likely due to compaction. Multiple index points indicate RSL was between -1 and -2 m at ~4.0 ka BP. One basal index point indicates that RSL rose to ~-1.4 ± 0.7 m at ~2.5 ka BP. Scatter in the index points increases during the last 2.0 ka and the large error bars did not allow us to satisfactorily reconcile the RSL history during this period. However, the youngest index point places the RSL at -0.4 ± 0.6 m at ~0.6 ka BP. A younger limiting point constrains the RSL to below -0.3 m at ~0.3 ka BP.

5.17 Northeastern Adriatic Sea (#17)

The RSL database for the northeastern Adriatic Sea is composed of 28 index points and 6 limiting points (figure 10, #17). Data come from marsh and lagoon cores near Trieste, on the Istrian coast and on Pag Island. Offshore cores undertaken during geological and geo-archaeological surveys in the Gulf of Trieste and on the Istrian coast provided additional index and limiting points. The oldest limiting point places the RSL below -28 m at 10.9 ka BP. During the early Holocene, multiple intercalated index and limiting points indicate that RSL was between -28 and -23 m between 10 and 9.6 ka BP. However, one basal index point places the RSL at -22 ± 1.2 m at ~9.6 ka BP. In the mid-Holocene, two basal index points constrain the RSL to -2.9 ± 1.0 m at ~5.0 ka BP. At ~3.1 ka BP one intercalated index point from Trieste placed the RSL at -0.2 ± 0.9 m while a coeval basal index point from the Istrian coast places the RSL at -1.29 ± 1.1 m. At ~2.0 ka BP multiple archaeological index and limiting points place the RSL between -1.75 and -1.4 m. In the northern part of the Gulf of Trieste, the archaeological data are in agreement with a lagoonal index point

759 placing the RSL at -1.0 ± 1.1 m at ~1.9 ka BP. Younger records indicate RSL has been within ~-0.5 of
760 modern MSL during the last ~1.5 ka BP.

761 ## 5.18 Northwestern Adriatic Sea (#18)

762 The database for the northwestern Adriatic Sea is composed of 40 index points and 9 limiting points. Data
763 derive from cores collected on the southern part of the Po Delta, near Comacchio and on the Romagna
764 coastal plain (figure 10, #18).
765 RSL is well constrained in the early to mid Holocene. By contrast, few data are available for the late
766 Holocene. The oldest index points place the RSL at -53.1 ± 1.0 m at ~12.9 ka BP. A suite of index points
767 indicate that RSL rose to ~-42.0 m at ~12.2 ka BP. Younger data show scatter, most likely related to the
768 variability in subsidence rates driven by the sediment compaction. However, a suite of basal index points
769 indicates a rapid rise in RSL in the remaining part of the early Holocene. RSL was at -23.4 ± 0.8 m at ~10 ka
770 BP, at -20.2 ± 0.9 m at ~9.2 ka BP, and at -15.1 ± 1.4 m at ~8.2 ka BP. Mid-Holocene index points indicate a
771 continuous rise in RSL that, at ~7.1 ka BP and at ~6.0 ka BP, was at -8.3 ± 1.4 m and at -7.7 ± 0.8 m,
772 respectively. Between 5 and 4.5 ka BP, limiting points constrain the RSL below -4.1 and above -4.6 m.
773 There is a lack of data-points between 4.5 and 1.8 ka BP. Younger basal index points indicate a RSL
774 stillstand at ~-2.8 m between ~1.7 and ~1.2 ka BP. The younger intercalated index point suggests RSL was
775 still at -2.7 ± 0.7 m at ~0.8 ka BP.

776 ## 5.19 Mid-eastern Adriatic Sea (#19)

777 The RSL history of the mid-western Adriatic Sea is restricted to the last ~2.6 ka BP. The database is
778 composed of 23 index points and 1 limiting point. Data come from *Lythophyllum byssoides* samples and
779 archaeological surveys performed on the islands of Vis and Bisevo in Croatia (figure 11, #19). The oldest
780 index point places the RSL at -1.5 ± 0.3 m at ~2.6 ka BP. One archaeological index point indicates that RSL
781 rose to -1.1 ± 0.3 m at ~1.9 ka BP. Multiple index points place the RSL at -0.7 ± 0.3 m between ~1.4 and
782 ~1.1 ka BP and at -0.3 ± 0.3 m between ~0.6 and ~0.2 ka BP.

5.20 Mid-western Adriatic Sea (#20)

The RSL history for the mid-western Adriatic Sea (figure 11, #20) is composed of 3 index points and 3 limiting points from the coastal plain of Pescara and the lower Sangro river valley. At ~10.4 ka BP, RSL was lower than -18.6 m. The oldest intercalated index point places the RSL at -11 ± 0.6 m at ~7.7 ka BP. RSL rose to -7.4 ± 1.1 m at ~7.7 ka BP. A lack of index points did not allow us to properly assess the RSL in the last ~7.5 ka BP. The youngest limiting point indicates that RSL was above -3 m ~2.5 ka BP.

5.21 Northern Apulia (#21)

The RSL history spans the mid to late Holocene. The database comprises 16 index points and 3 limiting points from cores in Battaglia coastal lake and Frattarolo marsh as well as from offshore cores in Gulf of Manfredonia (figure 11, #21). The oldest limiting point place the RSL above -14 m at ~7.7 ka BP. Multiple index points indicate RSL was at ~-6.0 m at ~6.8 ka BP. There is a scatter in the younger mid-Holocene index points, most likely due to compaction. At ~4.4 ka BP, RSL was at -2.2 ± 1.0 m. Then, multiple index points indicate RSL rose to ~-1.5 m. Younger index and limiting points, most likely affected by compaction, indicate that RSL rose to within ~2 m of modern MSL from ~2.6 ka BP to present.

5.22 Southern Apulia (#22)

The database is composed of 4 index points and 6 limiting points from lagoon cores in Alimini coastal lake and archaeological surveys carried out in the ancient towns of Egnazia and the Salento coast (figure 11, #22). The RSL history is restricted to the mid to late Holocene. At ~5.5 ka BP, RSL was at -4.0 ± 0.5 m. Then RSL rose to -3.4 ± 0.5 m at ~5.5 ka BP ~4.0 ka BP. Between ~4.0 and ~3.0 ka BP, RSL remained below ~-2.5 m. At ~2.0 ka BP, one intercalated index point places the RSL at -2.2 ± 0.7 m. RSL was still at -1.6 ± 1.0 m at ~1.0 ka BP.

6. Discussion

6.1 Standardization of the database and its applicability

We reconstructed the RSL histories of the western Mediterranean using an innovative multi-proxy standardization methodology based on: (1) modern taxa assemblages in Mediterranean lagoons and marshes;

808 (2) beachrock characteristics (cement fabric, chemistry and sedimentary features); and (3) the modern
809 distribution of Mediterranean fixed biological indicators on rocky coasts. We further added sea-level data
810 derived from archaeological coastal structures (Auriemma and Solinas, 2009; Morhange and Marriner,
811 2015). Results indicate a generally good match between the different proxies in most of the regions included
812 in the database. For example, in southern France there is very good agreement between the lagoonal index
813 points and the virtually incompressible samples (i.e. *L. byssoides* and archaeological index points, figure
814 12A) for the last 2 ka. Similarly, lagoonal and beachrock index points are in good agreement with terrestrial
815 and marine limiting points in documenting the RSL fall after the mid-Holocene highstand in southern
816 Tunisia (figure 12B). At the basin scale, compaction free index points are above those samples that may have
817 experienced compaction processes (figure 5A). Most basal index points have ages comprised between 7 and
818 5 ka BP (figure 5A), corresponding to the global slowdown in rates of rise and the onset of major coastal
819 progradation (Anthony et al., 2014; Lambeck et al., 2014).
820 A major issue in sea-level studies is to understand how small scale relative sea-level changes are manifest in
821 coastal sedimentary sequences (e.g., Kemp et al., 2011; Gehrels and Shennan, 2015). In our database, marsh
822 and lagoonal index points represents the majority of data. However, the vertical error bars of these index
823 points remain too large to capture sub-millennial RSL variability in the microtidal setting of the
824 Mediterranean Sea. To this end, methodological developments of the transfer function (e.g. Juggins and
825 Birks, 2012) offer the potential for high-resolution sea-level reconstructions (e.g., Gehrels, 2000; Kemp and
826 Telford, 2015). The identification of small-scale bio-stratigraphic changes from coastal sedimentary
827 sequences and the development of regional predictive plant zonation-, foraminifera- and/or ostracod-based
828 transfer functions to reconstruct former sea-levels are seldom reported in the Mediterranean (e.g., Anadòn et
829 al., 2002; Silvestri et al., 2005; Triantaphyllou et al., 2005). This is mainly due to the microtidal setting of
830 most Mediterranean coasts, which is not conducive to establishing a well-defined intertidal zoning. However,
831 our results indicate the potential of inner or semi-enclosed lagoon samples as RSL index points in the
832 Mediterranean Sea. In this database, we assigned an indicative range of 0 to -1 m MSL to these samples, on
833 the basis of the available literature. Future development of local or regional transfer functions could
834 significantly reduce this vertical uncertainly, possibly making them a high-resolution RSL indicator.

Our compilation underlines the importance of *L. byssoides* fossil rims as sea-level index points in the Mediterranean. The majority of our samples, collected at the beginning of the 1990s, show a large chronological error bar due to ^{14}C dating uncertainty. Recent developments in AMS techniques, pretreatment and calibration (e.g., Bronk Ramsey, 2008) could drastically reduce these uncertainties (e.g., Faivre et al., 2013).

Mediterranean beachrocks can be considered precise indicators when they are corroborated by chemical and fabric information of the cement and, when possible, by the description of sedimentary structures (Mauz et al., 2015b). Without such information, the resolution of beachrocks index points decreases considerably, making them a weak proxy for Mediterranean sea-level reconstruction. As an example, in southwestern Sardinia (#8), the large error bars of the youngest beachrock index point did not significantly improve the late Holocene RSL history of the region (figure 12C). Microstratigraphic analysis of the cement of these samples may lead to a considerable reduction in the error bar and, therefore, result in a better understanding of the RSL changes in this area.

Our database further confirmed the importance of archaeological RSL data-points. We decided to only produce index points from coastal structures closely related to former sea-level (i.e. fishtanks, fish ponds and ancient harbour interface structures such as quays and jetties). When coupled with fixed biological indicators, these structures may produce index points with uncertainty only represented by the leveling and the tidal errors (Morhange and Marriner, 2015). Conversely, we produced limiting points with such coastal structures whose relation with former sea-level is less clear (i.e. coastal quarries, roads, tombs, wrecks, sewage).

Our multi-proxy approach provides new insights into the ongoing debate about sea-level position during Roman times in the Tyrrhenian Sea. Fish tank interpretations by Evelpidou et al. (2012) place RSL between -0.58 and -0.32 m MSL while Lambeck et al.'s (2004b) interpretation places RSL between -1.37 and -1.2 m. On the Tiber Delta, Goiran et al., (2009, 2010) placed the RSL at -0.8 ± 0.2 m MSL at ~2.0 ka BP on the basis of the fixed biological indicators found in the Roman habour of Claudius' basin and the Darsena (figure 7, #9). One salt-marsh index point from the Tiber Delta indicates RSL was at -0.6 ± 0.6 m at ~1.9 ka BP (Di Rita et al., 2010). Long term uplift rates of ~0.11 mm a^{-1} are reported in the Tiber Delta area (Ferranti et al., 2010; Marra et al., 2013). If we apply the uplift correction to the two latter data-points we obtain a

RSL of between -0.8 and -1 m MSL during Roman times. This value is similar (with errors) to the Roman RSL obtained in the Gulf of Gaeta (#10). Here, one lagoonal index point places the RSL at -1 ± 0.5 m at 2.1 ka BP. In summary, our database seems to suggest that RSL rose to within 1 m of modern MSL from ~2.0 ka BP to present. Nonetheless, the associated error bars do not allow us to reconcile the different functional and architectural interpretations of Roman fish tanks. Further high-resolution studies are required in this area, if possible that couple fixed biological indicators and archaeological coastal structures.

6.2 Predicted vs observed RSL changes in the western Mediterranean

There is a generally good qualitative agreement between the predicted and the observed RSL changes. In regions where the record extends from the early Holocene, the database documents rapid rising rates (≤ 8 mm a^{-1}) between ~12 and ~7.5 ka BP corresponding to the major deglaciation phase (e.g., Peltier, 2004; Lambeck et al., 2014). Rising rates significantly slowed in the remaining part of the mid-Holocene and reached values <1 mm a^{-1} during the late Holocene where ice equivalent meltwater input is negligible (Milne et al., 2005; Church et al., 2008). Comparison between predicted and observed RSL changes are only robust at those sites where the RSL reconstruction is mainly based on virtually incompressible and basal data points. Conversely, caution is required for comparisons done with RSL reconstructions based only on intercalated samples.

The database documents a general overestimation of the nominal ICE-5G (VM2) model prediction in most of the regions. This is not surprising since the ICE-5G (VM2) model was not constrained by RSL observations from far-field sites with respect to the formerly glaciated regions (Peltier, 2004), such as the Mediterranean Sea. Data from most of the regions located in the northwestern sectors of our database (#2, #3, #4, #5, #6, figure 6 and 7) and from northwestern Sicily (#12, figure 9) are in good agreement with the lower boundary of the predicted curve (i.e. between nominal and minimal, see section 4, table 2). Disparities increase eastwards and southwards where the minimal curve slightly overestimates the RSL position, notably in the Ionian and mid to southern Adriatic Seas (figure 9, #14 and figure 11).

Such underestimation is also visible in regions considered tectonically stable. However, sediment compaction cannot account for this misfit. For instance, the underestimation is also present in the mid-eastern Adriatic region where the database is only composed of virtually incompressible samples (figure 11,

#19). It is possible that the chronology of the GIA model adopted in this study (and its rheological profile) could be modified in order to provide a better fit with the new RSL index points. However, we did not pursue this goal, since modifying these parameters would probably disrupt the agreement between the RSL observations available from polar regions and modelling predictions. This would require the implementation and the adoption of a fully 3D GIA model accounting for the lateral variations in viscosity, between the shield area and the remote sites, which is not the purpose of this study.

In our database, we avoided RSL reconstructions in areas affected by major tectonic deformation such as the Calabrian arc (see section, 2.1, Ferranti et al., 2006; Antonioli et al., 2009). However, comparison between predicted and observed RSL gave new insights into the influence of mild but significant long-term uplift on the sea-level history of a number regions. In mid-eastern Siciliy (region #13) our record agreed, using a larger dataset, with the results of previous studies (Dutton et al., 2009; Spampinato et al., 2011) that are consistent with long-term uplift rates of between ~0.4 and ~0.7 mm a^{-1}. In the western Ligurian Sea (region #4), the Holocene data-points collected near Nice describe a RSL history higher than those of the remaining areas of the region. The elevation of these data suggests that the low long-term uplift (average rate ≤0.06 mm a^{-1} since the last interglacial) reported by Dubar et al., (2008) has been active for more than half of the Holocene because these data are above the nominal curve from ~12.5 to ~5.5 ka BP. Our compilation confirms that such an uplift trend is restricted to the Nice area and rapidly decreases in the surrounding sectors, as already hypothesized on the basis of the MIS 5e elevations (Dubar et al., 2008; Rovere et al., 2011). Similarly, in the Tiber Delta (region #9) and on the Sele coastal plain (region #11) the long-term uplift rates reported by Ferranti et al., (2006; 2010) most likely control the position of RSL data points, especially for the early-to mid-Holocene. The offset between predictions and observations in central Spain (figure 6, #1) remains an open issue. Here, the early to mid-Holocene RSL data-points placed above the nominal curve suggest an underestimation of the RSL position by the ICE- 5G (VM2) isostatic model. At ~8.3 ka the RSL was ~6 m higher than in northern Spain (figure 6, #1). On-going vertical movements (Serpelloni et al., 2013) do not exceed ±0.5 mm a^{-1} with slightly higher subsidence rates (< 2 mm a^{-1}) near Valencia (figure 2); these data meant that it was difficult to robustly support a tectonic component in the current elevation of the index points. However, the RSL record in this region is based on a restricted number

of index and limiting points and further investigations are required to better assess the mid to late-Holocene evolution of this area.

Furthermore, our database indicates that the major western Mediterranean subsidence trends are recorded in the Ebro Delta and the northwestern Adriatic Sea. The comparison between the elevation of the index points from the Ebro Delta and the predicted RSL changes (figure 6, #2) indicates subsidence rates of ~1 mm a^{-1} between ~6.0 and ~3.5 ka BP, rising to ≥ 2 mm a^{-1} during the last ~2.5 ka BP. This subsidence pattern is chiefly controlled by the increase in sediment loading following the RSL stabilization at ~7.0 ka BP. The increasing subsidence rates recorded in the last ~2.5 ka BP are most likely linked to the transition from estuarine to deltaic environments at the river-mouth (Trincardi and Maselli, 2013; Anthony et al., 2015) with a consequent increase of sediment loading. Furthermore, recent studies in Mediterranean deltaic contexts have revealed a negative correlation between subsidence rates and time, translating the rapid compaction of the latest Holocene deposits. Compaction rates progressively decline with the increasing age of sediments (Marriner et al., 2012a). The mechanistic explanation for this pattern appears consistent with the rapid compaction of the youngest delta sediments that undergo the most important phase of volume loss, through dewatering and oxidation of organic material, during earlier periods following deposition (Becker and Sultan, 2009).

Our data corroborated, using a larger dataset, the general subsidence trend in the northwestern portion of the Adriatic Sea (figure 10, #16, #18) already reported by Antonioli et al., (2009). South of the Po Delta, the observed subsidence is the sum of sediment compaction and long-term negative vertical motions related to the neotectonic framework of the area (e.g., Ferranti et al., 2006; Antonioli et al., 2009). Comparison between the elevation of basal and intercalated index points from the same area (and thus with comparable tectonics), gives insights into the compaction-related subsidence. We attempted this comparison in Codigoro and Comacchio (appendix A, Cibin and Stefani, 2009; Sarti et al., 2009) and the calculated subsidence rates are ~0.5 mm a^{-1} for the last ~9.5 ka BP.

Human-induced subsidence explains the significant scatter in the index points from Venice lagoon (region #16, figure 10) especially during the last 2.0 ka (Serandrei-Barbero et al., 2006; Antonioli et al., 2009). In general, an assessment of the variability in subsidence trends in the northwestern sector of the Adriatic Sea is challenging. A comparative study, using de-compacted coring data, long-term vertical movements and the

946 geometry of local faults would significantly improve the understanding of the Holocene RSL evolution of
947 this area.
948 There is a small shift in the RSL curve between the eastern border of the Rhone Delta and the remaining sites
949 of southern France (region #3, figure 6). The Rhone river shows major progradation rates (≥150 m a^{-1})
950 during the last 1.7 ka BP leading to significant sediment loading, especially on the eastern part of the delta
951 (Maselli and Trincardi, 2013). However, some localized tectonic subsidence has been evoked as a cause for
952 this peculiar RSL pattern (Vella and Provansal, 2000; Vella et al., 2005). These authors excluded
953 compaction-related subsidence because most of the index points are basal peat samples that directly overlie
954 the uncompressible Pleistocene substratum. Nonetheless, whether it is local tectonics or major sediment
955 loading that has caused the subsidence, the eastern Rhone data-points are not indicative of the RSL history of
956 southern France.
957 An intriguing open issue is represented by the RSL history of region #7 (northern Sardinia and southern
958 Corsica, figure 7) and #8 (southwestern Sardinia, figure 8). Here, both lagoonal and beachrock index points
959 are placed significantly below the minimal predicted curve, especially for the mid-Holocene. Both islands
960 are considered to have been tectonically stable since the last interglacial (Ferranti et al., 2006) and ongoing
961 vertical movements are negligible (Serpelloni et al., 2013). As for the mid-southern Adriatic and Ionian Seas,
962 the underestimation of the isostatic contribution in this area may be a good explanation for the misfit
963 between RSL index points and the predicted curve. However, in the early and mid Holocene, the sole index
964 point from Is Mistras closely matches the RSL prediction (figure 8, #8) while lagoonal index points from
965 Cagliari and Oristano (Antonioli et al., 2007) are significantly lower than the minimal predicted curve. Such
966 a misfit could be related to some dating problems (both in Is Mistras and in Cagliari) or with compaction
967 (even if the early Holocene record is based on beachrocks and basal samples). At the moment, we cannot
968 robustly assess the mid to early Holocene RSL history in this sector of the western Mediterranean and
969 additional datapoints are required.
970 Similarly, in region #7, beachrock samples (virtually incompressible) are found significantly lower than the
971 predicted curve, between ~2 and ~7.1 ka BP. Here, the magnitude of the misfit (significantly greater than the
972 remaining regions, especially in the Tyrrhenian Sea) calls for alternative explanations mainly focused on the
973 quality of the RSL data-points. Disparities arising from radiocarbon dates of beachrock bulk cement are not

974 unusual (e.g., Vousdoukas et al., 2007), especially for samples during the early 1980s (like most of the
975 beachrock of this region, Nesteroff, 1984). Results of recent coring in the Gulf of Sagone (mid-eastern
976 Corsica) placed the RSL above -2.7 m MSL at ~3.8 ka BP and indicate that sea-level rise in the last ~2.5 ka
977 BP was within 1 m (Ghilardi, 2015). These data suggest RSL was significantly higher than the one indicated
978 by the beachrock samples, at least during the late Holocene.
979 As stated at the beginning of this section, the combined effects of glacio and hydro isostatic components in
980 the western Mediterranean resulted in a continuous rise in RSL during the Holocene.
981 The sole exception is represented by the mid-Holocene highstand in southern Tunisia (Gulf of Gabes) that,
982 according to our record, occurred between ~6.0 and ~5.0 ka BP and did not exceed 1.5 m above MSL.
983 However, Morhange and Pirazzoli (2005), on the basis of ^{14}C dating of a subtidal shell (*Petricola* sp.) and
984 vermetus (*Vermetus triqueter*), suggest a highstand at ~1.9 m during the same period. More recently, OSL
985 dating of a beachrock outcrop in the Gulf of Gabes suggested a RSL at 1.4 ± 0.4 m MSL at ~6.0 ka BP
986 (Mauz et al., 2015a). This estimate, coupled with our result, seems to suggest that the magnitude proposed by
987 Morhange and Pirazzoli (2005) is slightly overestimated and may be affected by levelling errors with respect
988 to the biological MSL.
989 Both the absence of significant historical seismicity and the long-term tectonic stability (figure 2) suggest
990 that the southern Tunisia high-stand is purely of isostatic origin (Stocchi et al., 2009; Mauz et al., 2015a).
991 The geomorphology of the inner part of the Gulf of Gabes and the continental levering effects (e.g. the
992 extensive upward deflection of continental interiors and the broad subsidence of ocean basin, Mitrovica and
993 Milne, 2002) play a key role in the occurrence of this highstand. In fact, due to the wide and shallow (≤30 m
994 depth) continental shelf (Sammari et al., 2006), the inner part of the Gulf of Gabes acts as a pure continental
995 margin where the levering effects are not counterbalanced by the ocean loading. Thus, the subsidence driven
996 by the water loading in the remaing part of the western Mediterranean is not able to offset the highstand in
997 this region.
998 The timing of this highstand (~5.5 ka BP) suggests a negligible role of Northern hemisphere ice sheets due to
999 the mutual cancellation of the meltwater contributions from the Laurentide and Fennoscandian ice sheets
1000 after ~7 ka BP (Stocchi and Spada, 2007; Stocchi et al., 2009). Conversely, our record improved and refined
1001 the RSL reconstruction provided by Stocchi et al., (2009) and Mauz et al., (2015a) confirming that the

1002 Tunisian high-stand is compatible with the melting history of the remote Antarctica ice sheet (Bentley, 1999;
1003 Stocchi and Spada, 2007; Stocchi et al., 2009).
1004
1005 6.3 RSL variability along the Western Mediterranean basin
1006 In order to better assess the spatial variability of Holocene RSL changes along the western Mediterranean
1007 basin, we tried to minimize both the local vertical movements and the effects of compaction in our database.
1008 For this reason, figure 13A,C only depicts the index points collected at sites: (i) with long-term vertical
1009 movements $\leq$0.06 mm a^{-1} (figure 2, MIS 5e); (ii) with ongoing vertical motions between -0.5 and 0.5 mm a^{-1}
1010 (figure 2, GPS); and (iii) not affected by significant compaction-related subsidence (e.g., the Ebro Delta) or
1011 local fault activity (e.g. the Var fault).
1012 With the sole exception of southern Tunisia, the data indicate a continuous rise in RSL which, at the basin
1013 scale, rose by ~45 m in ~12 ka (figure 13A).
1014 Even if affected by scatter, the data show a general slowdown in western Mediterranean sea-level rise
1015 starting from ~7.5 ka BP, consistent with the final phase of the North American deglaciation (e.g., Carlson et
1016 al., 2008; Lambeck et al., 2014) followed by a further decrease in rising rates related to the progressive
1017 reduction in meltwater input (e.g., Peltier and Tushingham, 1991; Milne et al., 2005).
1018 Comparatively, the late Holocene record (i.e. the last 4 ka BP) is affected by less scatter. In this period, ice
1019 equivalent meltwater input is negligible (Peltier, 2004; Milne et al., 2005; Church et al., 2008). Therefore,
1020 once tectonics and sediment compaction are factored out, any change observed in RSL is entirely related to
1021 vertical land movements due to GIA (e.g., Engelhart et al., 2009; 2015). According to Engelhart et al., 2009,
1022 we calculated the late Holocene RSL rising rates excluding the 20th century sea-level contribution and thus
1023 expressing all our data with respect to MSL at A.D. 1900 (figure 13B). We further excluded for this analysis
1024 the southern Tunisia index points describing a RSL history not comparable with the other datasets in our
1025 study area (see section 6.2). Thus, the late Holocene record in figure 13B most likely encompasses the total
1026 variability in isostatic contribution in the western Mediterranean. Our estimates indicate that GIA-related
1027 land movements in the western Mediterranean vary between ~3.4 m in the southeastern part of the basin up
1028 to ~1.6 m in the northwest. The latter value is mainly derived from region #14 and #22, where the Holocene

1029 record is only based on intercalated index points. For this reason, assessment of any possible role of
1030 compaction in the late Holocene was not possible with the present dataset.
1031 Preliminary analysis of the normal distribution of late Holocene rising rates (figure 4D) shows that values
1032 ranging between 0.55 and 0.20 mm a^{-1} are the most represented along the Mediterranean coast. Rates
1033 increase up to ~0.85 mm a^{-1}, but caution should be used in using these values because a possible compaction
1034 influence cannot be excluded in some dataset from the southeastern sector of the western Mediterranean Sea
1035 (see above).
1036 The figure 13D clearly shows that late Holocene sea-level rising rates are slower than those recorded by
1037 most of the Mediterranean tide gauges (table 3) but still account for at least the 25-30% of the rate.
1038 Therefore, for better understanding of current rates of Mediterranean sea-level rise from tide gauges,
1039 correction for GIA is required (e.g., Engelhart et al., 2009; Church and White, 2011). Site-specific
1040 assessment of the GIA signal in the western Mediterranean is beyond the scope of this paper. However,
1041 future application of spatio-temporal statistical models (e.g., Parnell et al., 2011; Engelhart et al., 2015;
1042 Parnell and Gehrels, 2015) to the Mediterranean RSL data may provide a long-term baseline against which
1043 to gauge changes in sea-level during the 20th century (e.g., Engelhart et al., 2009; Kemp et al., 2011; Gehrels
1044 and Woodworth, 2013) and provide a framework for more accurate 21st century sea-level predictions (e.g.
1045 Church and White, 2011; Horton et al., 2014).

1046 7. Conclusions

1047 In this paper, we reviewed 918 radiocarbon-dated RSL proxies using, for the first time in the Mediterranean
1048 basin, a standardized protocol to produce RSL index and limiting points. This allowed us to compare and
1049 contrast data from different literature sources in order to obtain basin-scale insights into the processes
1050 driving Holocene RSL changes. The database in appendix A is dynamic and future users can add further data
1051 or subdivide the data points on the basis of other criteria. Moreover, future RSL reconstructions carried out
1052 using this standardized methodology will produce homogeneous and comparable RSL data rendering the
1053 assessment of RSL variability in the Mediterranean much easier.
1054 Our quality-controlled database has an excellent temporal coverage, allowing a robust reconstruction of RSL
1055 changes since 14 ka BP. By contrast, the spatial coverage is significantly affected by a paucity of RSL data

1056 from the southern coast of the Mediterranean. Therefore, future sea-level investigations in Algeria, Morocco
1057 and particularly Libya (a key site for tuning the global eustatic signal, e.g., Mitrovica and Milne, 2008) are a
1058 key priority. Thanks to the very local RSL highstand of the Gulf of Gabes, we were able to detect the
1059 influence of the remote Antarctic ice sheet on the Mediterranean RSL history. In the remaining part of
1060 western Mediterranean, GIA (glacio- and hydro-) induced subsidence that prevented the occurrence of this
1061 highstand, with a continuous rise in RSL for the whole Holocene. Our data indicate a sudden slowdown in
1062 the rising rates at ~7.5 ka BP and a further deceleration during the last ~4.0, where any observed changes are
1063 related to variability in GIA or neotectonics.
1064 Precise estimates of Mediterranean sea-level rise in the pre-satellite era are essential for accurate 21st century
1065 sea-level predictions, but the use of tide-gauge records is complicated by the contributions from changes in
1066 land level due to GIA. In this paper, we provide a preliminary quantification of the on-going GIA
1067 contribution in the western Mediterranean that, at least in the northwestern sector, accounts for the 25-30%
1068 of the on-going rising rates recorded by the tidal gauges. In the southeastern sector, our results weakly
1069 constrained the GIA contribution because the sole presence of intercalated index points did not allow for a
1070 robust late Holocene RSL reconstruction. Improvement of this dataset and future applications of spatio-
1071 temporal statistical techniques are required for site-specific estimates of the isostatic contribution and for the
1072 consequent improved assessment of 20th century acceleration of Mediterranean sea-level rise.

1073 *8. Acknowledgments*

1074 This work has carried out thanks to the support of the Labex OT-Med (ANR-11-LABX-0061) and of the
1075 A*MIDEX project (n°ANR-11-IDEX-0001-02), funded by the «Investissements d'Avenir» program of the
1076 French National Research Agency (ANR). This compilation of the database was motivated by discussions at
1077 the workshops of Medflood, INQUA project n. 1203 and PALSEA (PAGES/INQUA/WUN working group).
1078 GS has been supported by the DiSBeF grant n. CUP H31J13000160001. AR's research is funded by the
1079 Institutional Strategy of the University of Bremen, German Excellence Initiative, and by ZMT Center for
1080 Tropical Marine Ecology.
1081 MV would like to thank Prof. Ben Horton (Sea Level Research, Rutgers University, USA), Prof. Eduard
1082 Bard (Collège de France-CEREGE, France) and Prof. Bruno Hamelin (Aix Marseille Université-CEREGE,

France) for the fruitful discussions. We thank Veronica Rossi (University of Bologna, Italy), Stefano Furlani (University of Trieste, Italy), Pilàr Carmona-Gonzàles (University of Valencia, Spain), Matthieu Ghilardi (CNRS-CEREGE, France), Marco Firpo and Pierluigi Brandolini (University of Genova, Italy), Daniela Pantosti and Paolo Marco De Martini (INGV Rome, Italy) for their help in compilation of the database and the definition of the indicative meanings. The constructive comments of the associate editor I. Candy and of the two anonymous reviewers significantly improved an earlier version of the paper.

9. References

Ambert, P. 1999. Les formations littorales Pléistocènes du Languedoc. Quaternaire 10, 83-93.

Amorosi, A., Dinelli, E., Rossi, V., Vaiani, S. C., Sacchetto, M. 2008a. Late Quaternary palaeoenvironmental evolution of the Adriatic coastal plain and the onset of Po River Delta. Palaeogeography, Palaeoclimatology, Palaeoecology 268(1), 80-90.

Amorosi, A., Fontana, A., Antonioli, F., Primon, S., Bondesan, A. 2008b. Post-LGM sedimentation and Holocene shoreline evolution in the NW Adriatic coastal area. GeoActa 7, 41-67.

Amorosi, A., Rossi, V., Vella, C. 2013. Stepwise post-glacial transgression in the Rhône Delta area as revealed by high-resolution core data. Palaeogeography, Palaeoclimatology, Palaeoecology 374, 314-326.

Amorosi, A., Ricci Lucchi, M., Rossi, V., Sarti, G. 2009. Climate change signature of small-scale parasequences from Lateglacial–Holocene transgressive deposits of the Arno valley fill. Palaeogeography, Palaeoclimatology, Palaeoecology 273(1), 142-152.

Anadón, P., Gliozzi, E., Mazzini, I. 2002. Paleoenvironmental reconstruction of marginal marine environments from combined paleoecological and geochemical analyses on ostracods. In: Holmes J., Chivas A. (Eds.), The Ostracoda: Applications in Quaternary Research, Geophysical Monograph, vol. 131, pp. 227–247.

Anthony, E.J., Marriner, N., Morhange, C. 2014. Human influence and the changing geomorphology of Mediterranean deltas and coasts over the last 6000years: From progradation to destruction phase? Earth-Science Reviews 139, 336-361.

Antonioli, F., Anzidei, M., Lambeck, K., Auriemma, R., Gaddi, D., Furlani, S., Orrù P., Solinas, E., Gaspari, A., Karinja , S., Kovacic, V., Surace, L. 2007. Sea-level change during the Holocene in Sardinia and in the northeastern Adriatic (central Mediterranean Sea) from archaeological and geomorphological data. Quaternary Science Reviews, 26(19), 2463-2486.

1113 Antonioli, F., Chemello, R., Improta, S., Riggio, S. 1999. The Dendropoma (Mollusca Gastropoda,
1114 Vermetidae) intertidal reef formations and their paleoclimatological use. Marine Geology 161, 155-170.

1115 Antonioli, F., D'Orefice, M., Ducci, S., Firmati, M., Foresi, L. M., Graciotti, R., Principe, C. 2011.
1116 Palaeogeographic reconstruction of northern Tyrrhenian coast using archaeological and geomorphological
1117 markers at Pianosa island (Italy). Quaternary International 232(1), 31-44.

1118 Antonioli, F., Ferranti, L., Fontana, A., Amorosi, A., Bondesan, A., Braitenberg, C., Dutton, A., Fontolan,
1119 G., Furlani, S., Lambeck, K., Mastronuzzi, G., Monaco, C., Spada, G., Stocchi, P. 2009. Holocene relative
1120 sea-level changes and vertical movements along the Italian and Istrian coastlines. Quaternary International
1121 206(1), 102-133.

1122 Antonioli, F., Lo Presti, V., Rovere, A., Ferranti, L., Anzidei, M., Furlani, S., Mastronuzzi, G., Orrù, P.,
1123 Scicchitano, G., Sannino, G., Spampinato C.R., Pagliarulo, R., Deiana, G., de Sabata, E., Sanso P., Vacchi,
1124 M., Vecchio, A. (2015). Tidal notches in Mediterranean Sea: a comprehensive analysis. Quaternary Science
1125 Reviews, 119, 66-84.

1126 Anzidei, M., Antonioli, F., Lambeck, K., Benini, A., Soussi, M., Lakhdar, R. 2011. New insights on the
1127 relative sea level change during Holocene along the coasts of Tunisia and western Libya from archaeological
1128 and geomorphological markers. Quaternary International 232(1), 5-12.

1129 Anzidei, M., Lambeck, K., Antonioli, F., Furlani, S., Mastronuzzi, G., Serpelloni, E., Vannucci, G. 2014.
1130 Coastal structure, sea-level changes and vertical motion of the land in the Mediterranean. Geological
1131 Society, London, Special Publications 388(1), 453-479.

1132 Auriemma, R., Solinas, E. 2009. Archaeological remains as sea level change markers: a review. Quaternary
1133 International 206(1), 134-146.

1134 Bard, E., Hamelin, B., Arnold, M., Montaggioni, L., Cabioch, G., Faure, G., Rougerie, F. 1996. Deglacial
1135 sea-level record from Tahiti corals and the timing of global meltwater discharge. Nature 382(6588), 241-244.

1136 Bard, E., Hamelin, B., Delanghe-Sabatier, D. 2010. Deglacial meltwater pulse 1B and Younger Dryas sea
1137 levels revisited with boreholes at Tahiti. Science, 327(5970), 1235-1237.

1138 Becker, R.H., Sultan, M. 2009. Land subsidence in the Nile Delta: Inferences from radar interferometry: The
1139 Holocene 19, 949–954.

1140 Bentley, M.J. 1999. Volume of Antarctic ice at the Last Glacial Maximum, and its impact on global sea level
1141 change. Quaternary Science Reviews 18(14), 1569-1595.

1142 Blázquez, A. M., Usera, J. 2010. Palaeoenvironments and Quaternary foraminifera in the Elx coastal lagoon
1143 (Alicante, Spain). Quaternary International 221(1), 68-90.

1144 Billi, A., Faccenna, C., Bellier, O., Minelli, L., Neri, G., Piromallo, C., Presti, D, Scrocca, D., Serpelloni, E.
1145 2011. Recent tectonic reorganization of the Nubia-Eurasia convergent boundary heading for the closure of
1146 the western Mediterranean. Bulletin de la Société Géologique de France 182(4), 279-303.

1147 Bronk Ramsey, C. 2008. Radiocarbon dating: Revolutions in Understanding. Archaeometry 50(2), 249-275.

1148 Caldara, M., Caroli, I., Simone, O. 2008. Holocene evolution and sea-level changes in the Battaglia basin
1149 area (eastern Gargano coast, Apulia, Italy). Quaternary International 183(1), 102-114.

1150 Caldara, M., Simone, O. 2005. Coastal changes in the eastern Tavoliere Plain (Apulia, Italy) during the Late
1151 Holocene: Natural or anthropic? Quaternary Science Reviews 24(18), 2137-2145.

1152 Carboni, M. G., Bergamin, L., Di Bella, L., Esu, D., Cerone, E. P., Antonioli, F., Verrubbi, V. 2010.
1153 Palaeoenvironmental reconstruction of late Quaternary foraminifera and molluscs from the ENEA borehole
1154 (Versilian plain, Tuscany, Italy). Quaternary Research 74(2), 265-276.

1155 Carboni, M. G., Bergamin, L., Di Bella, L., Iamundo, F., Pugliese, N. 2002. Palaeoecological evidences from
1156 foraminifers and ostracods on Late Quaternary sea-level changes in the Ombrone river plain (central
1157 Tyrrhenian coast, Italy). *Geobios*, *35*, 40-50.

1158 Carboni, M. G., Succi, M. C., Bergamin, L., Di Bella, L., Frezza, V., Landini, B. 2009. Benthic foraminifera
1159 from two coastal lakes of southern Latium (Italy). Preliminary evaluation of environmental quality. Marine
1160 Pollution Bulletin 59(8), 268-280.

1161 Carlson, A.E., LeGrande, A.N., Oppo, D.W., Came, R.E., Schmidt, G.A., Anslow, F.S., Licciardi, J.M.,
1162 Obbink, E.A., 2008. Rapid early Holocene deglaciation of the Laurentide ice sheet. Nature Geoscience 1 (9),
1163 620-624.

1164 Carminati, E., Doglioni, C., Scrocca, D. 2003. Apennines subduction‐related subsidence of Venice (Italy).
1165 Geophysical Research Letters, 30(13).

1166 Carmona-González, P. C., Ballester, J.P. 2011. Geomorphology, geoarchaeology and ancient settlement in
1167 the Valencian Gulf (Spain). Méditerranée. Revue géographique des pays méditerranéens/Journal of
1168 Mediterranean geography (117), 61-72.

1169 Church, J. A., White, N. J., Aarup, T., Wilson, W. S., Woodworth, P. L., Domingues, C. M., Hunter, J.R.,
1170 Lambeck, K. 2008. Understanding global sea levels: past, present and future. Sustainability Science 3(1), 9-
1171 22.

1172 Church, J.A., White, N.J., 2011. Sea-Level Rise from the Late 19th to the Early 21st Century. Surveys in
1173 Geophysics 32 (4-5), 585-602.

1174 Cibin U., Stefani, M., 2009. Carta Geologica d'Italia alla scala 1:50.000. Foglio 187, Codigoro. Note
1175 illustrative. http://www.isprambiente.gov.it/Media/carg/note_illustrative/187_Codigoro.pdf

1176 Cimerman, F., Langer, M.R. 1991. Mediterranean Foraminifera. Slovenska Akademija Znanosti in
1177 Umetnosti, Ljubljana.

1178 Colombaroli, D., Marchetto, A., Tinner, W. 2007. Long-term interactions between Mediterranean climate,
1179 vegetation and fire regime at Lago di Massaciuccoli (Tuscany, Italy). Journal of Ecology, 95(4), 755-770.

1180 Correggiari, A., Roveri, M., Trincardi, F. 1996. Late Pleistocene and Holocene evolution of the north
1181 Adriatic Sea. Il Quaternario 9, 697-704.

1182 De Martini, P. M., Barbano, M. S., Smedile, A., Gerardi, F., Pantosti, D., Del Carlo, P., Pirrotta, C. 2010. A
1183 unique 4000year long geological record of multiple tsunami inundations in the Augusta Bay (eastern Sicily,
1184 Italy). Marine Geology 276 (1), 42-57.

1185 De Muro, S., Orrù, P. 1998. Il contributo delle Beach-Rock nello studio della risalita del mare olocenico. Le
1186 Beach-Rock post-glaciali della Sardegna nord-orientale. Il Quaternario, 11(1), 19-39.

1187 Deschamps, P., Durand, N., Bard, E., Hamelin, B., Camoin, G., Thomas, A. L., Yokoyama, Y. 2012. Ice-
1188 sheet collapse and sea-level rise at the Bolling warming 14,600 [thinsp] years ago. Nature 483(7391), 559-
1189 564.

1190 Desruelles, S., Fouache, É., Ciner, A., Dalongeville, R., Pavlopoulos, K., Kosun, E., Coquinot, Y., Potdevin,
1191 J. L. 2009. Beachrocks and sea level changes since Middle Holocene: comparison between the insular group
1192 of Mykonos–Delos–Rhenia (Cyclades, Greece) and the southern coast of Turkey. Global and Planetary
1193 Change 66(1), 19-33.

1194 Di Rita, F., Celant, A., Magri, D. 2010. Holocene environmental instability in the wetland north of the Tiber
1195 delta (Rome, Italy): sea-lake-man interactions. Journal of Paleolimnology 44(1), 51-67.

1196 Di Rita, F., Melis, R.T. 2013. The cultural landscape near the ancient city of Tharros (central West Sardinia):
1197 vegetation changes and human impact. Journal of Archaeological Science 40(12), 4271-4282.

1198 Dubar, M., Anthony, E. J. 1995. Holocene environmental change and river-mouth sedimentation in the Baie
1199 des Anges, French Riviera. Quaternary Research 43(3), 329-343.

1200 Dubar, M., Innocent, C., Sivan, O. 2008. Radiometric dating (U/Th) of the lower marine terrace (MIS 5.5)
1201 west of Nice (French Riviera): Morphological and neotectonic quantitative implications. Comptes Rendus
1202 Geoscience 340(11), 723-731.

1203 Dumas, B., Guérémy, P., Raffy, J. 2005. Evidence for sea-level oscillations by the “characteristic thickness”
1204 of marine deposits from raised terraces of Southern Calabria (Italy). Quaternary Science Reviews 24(18),
1205 2120-2136.

1206 Dupré, M., Fumanal, M. P., Sanjaume, E., Santisteban, C., Usera, J., 1988 Quaternary evolution of Pego
1207 coastal lagoon (Southern Valencia, Spain). Palaeogeography, Palaeoclimatology, Palaeoecology, 68, 291-
1208 299.

1209 Dura, T., Cisternas, M., Horton, B. P., Ely, L. L., Nelson, A. R., Wesson, R. L., Pilarczyk, J. E. 2014.
1210 Coastal evidence for Holocene subduction-zone earthquakes and tsunamis in central Chile. Quaternary
1211 Science Reviews 113, 93-111.

1212 Dutton, A., Lambeck, K., 2012. Ice volume and sea level during the last interglacial. Science 337 (6091),
1213 216–219.

1214 Dutton, A., Scicchitano, G., Monaco, C., Desmarchelier, J. M., Antonioli, F., Lambeck, K., Mortimer, G.
1215 2009. Uplift rates defined by U-series and 14 C ages of serpulid-encrusted speleothems from submerged
1216 caves near Siracusa, Sicily (Italy). Quaternary Geochronology 4(1), 2-10.

1217 Edwards, R. J. 2006. Mid-to late-Holocene relative sea-level change in southwest Britain and the influence
1218 of sediment compaction. The Holocene 16(4), 575-587.

1219 Engelhart, S. E., Vacchi, M., Horton, B. P., Nelson, A. R., Kopp, R. E. (2015). A sea-level database for the
1220 Pacific coast of central North America. Quaternary Science Reviews 113, 78-92.

1221 Engelhart, S.E., Horton, B.P., 2012. Holocene sea level database for the Atlantic coast of the United States.
1222 Quaternary Science Reviews 54, 12-25.

1223 Engelhart, S.E., Horton, B.P., Douglas, B.C., Peltier, W.R., Törnqvist, T.E., 2009. Spatial variability of late
1224 Holocene and 20th century sea-level rise along the Atlantic coast of the United States. Geology 37, 1115-
1225 1118.

1226 Evelpidou, N., Pirazzoli, P., Vassilopoulos, A., Spada, G., Ruggieri, G., Tomasin, A. 2012. Late Holocene
1227 sea level reconstructions based on observations of Roman fish tanks, Tyrrhenian Coast of Italy.
1228 Geoarchaeology 27(3), 259-277.

1229 Faccenna, C., Becker, T. W., Auer, L., Billi, A., Boschi, L., Brun, J.P., Capitanio, F.A., Funiciello, F.,
1230 Horvàth, F., Jolivet L., Piromallo, C., Royden, L., Rossetti, F., Serpelloni, E. 2014. Mantle dynamics in the
1231 Mediterranean. Reviews of Geophysics 52(3), 283-332.

1232 Faivre, S., Bakran-Petricioli, T., Horvatincic, N. 2010. Relative Sea-Level Change During the Late Holocene
1233 on the Island of Vis (Croatia)–Issa Harbour Archaeological Site. Geodinamica Acta 23(5-6), 209-223.

1234 Faivre, S., Bakran-Petricioli, T., Horvatinčić, N., Sironić, A. 2013. Distinct phases of relative sea level
1235 changes in the central Adriatic during the last 1500years—influence of climatic variations?.
1236 Palaeogeography, Palaeoclimatology, Palaeoecology 369, 163-174.

1237 Farrell, W.E., Clark, J.A. 1976. On post-glacial sea level. Royal Astronomical Society Geophysical Journal
1238 46, 647-657.

1239 Ferranti, L., Antonioli, F., Anzidei, M., Monaco, C., Stocchi, P. 2010. The timescale and spatial extent of
1240 vertical tectonic motions in Italy: insights from relative sea-level changes studies. Journal of the Virtual
1241 Explorer 36 (Paper 30).

1242 Ferranti, L., Antonioli, F., Mauz, B., Amorosi, A., Dai Pra, G., Mastronuzzi, G., Monaco, C., Orrù, P.E.,
1243 Pappalardo, M., Radtke, U., Renda, P., Romano, P., Sansò, P., Verrubbi, V. 2006. Markers of the last
1244 interglacial sea-level high stand along the coast of Italy: tectonic implications. Quaternary International 145,
1245 30-54.

1246 Ferranti, L., Monaco, C., Antonioli, F., Maschio, L., Kershaw, S., Verrubbi, V. 2007. The contribution of
1247 regional uplift and coseismic slip to the vertical crustal motion in the Messina Straits, Southern Italy:
1248 evidence from raised Late Holocene shorelines. Journal of Geophysical Research: Solid Earth (1978–2012),
1249 112(B6).

1250 Flemming, N.C. 1969. Archaeological evidence for eustatic change of sea level and earth movements in the
1251 western Mediterranean during the last 2,000 years. Geological Society of America Special Papers 109, 1-98.

1252 Furlani, S., Antonioli, F., Biolchi, S., Gambin, T., Gauci, R., Lo Presti, V., Anzidei, M., Devoto, S.,
1253 Palombo, M., Sulli, A. 2013. Holocene sea level change in Malta. Quaternary International 288, 146-157.

1254 Furlani, S., Biolchi, S., Cucchi, F., Antonioli, F., Busetti, M., Melis, R. 2011. Tectonic effects on Late
1255 Holocene sea level changes in the Gulf of Trieste (NE Adriatic Sea, Italy). Quaternary International 232(1),
1256 144-157.

1257 Geherls, W.R., Shennan, I. 2015. Sea level in time and space: revolutions and inconvenient truths. Journal of
1258 Quaternary Science 30(2), 131-143.

1259 Gehrels, W. R. 2000. Using foraminiferal transfer functions to produce high-resolution sea-level records
1260 from salt-marsh deposits, Maine, USA. The Holocene 10(3), 367-376.

1261 Gehrels, W. R., Woodworth, P. L. 2013. When did modern rates of sea-level rise start? Global and Planetary
1262 Change 100, 263-277.

1263 Gehrels, W.R., Long, A.J., 2007. Quaternary land-ocean interactions: sea-level change, sediments and
1264 tsunami. Marine Geology 242, 169-190.

1265 Gerardi, F., Smedile, A., Pirrotta, C., Barbano, M.S., De Martini, P.M., Pinzi, S., Gueli, A.M., Ristuccia,
1266 G.M., Stella, G., Troja, S.O. 2012. Geological record of tsunami inundations in Pantano Morghella (south-
1267 eastern Sicily) both from near and far-field sources. Natural Hazards and Earth System Sciences 12(4), 1185-
1268 1200.

1269 Ghilardi, M., 2015. Approche géoarchéologique des basses vallées fluviales de la Corse : la necessaire prise
1270 en compte de l'evolution paysagère au cours de l'Holocène. Rapport d'activités 2013-2014. Programme
1271 collectif de recherche (PCR 2013-2015). 112 pp.

1272 Goiran, J. P., Tronchère, H., Collalelli, U., Salomon, F., Djerbi, H. 2009. Découverte d'un niveau marin
1273 biologique sur les quais de Portus: le port antique de Rome. Méditerranée (1), 59-67.

1274 Goiran, J. P., Tronchère, H., Salomon, F., Carbonel, P., Djerbi, H., Ognard, C. 2010. Palaeoenvironmental
1275 reconstruction of the ancient habours of Rome: Claudius and Trajan's marine habours on the Tiber delta.
1276 Quaternary International 216(1), 3-13.

1277 Gravina, M.F., Ardizzone, G.D., Scaletta, F., Chimenz, C. 1989. Descriptive analysis and classification of
1278 benthic communities in some Mediterranean coastal lagoons (central Italy). Marine Ecology 10(2), 141-166.

1279 Hall, G.F., Hill, D.F., Horton, B.P., Engelhart, S.E., Peltier, W.R. 2013. A high-resolution study of tides in
1280 the Delaware Bay: Past conditions and future scenarios. Geophysical Research Letters 40,
1281 doi:10.1029/2012GL054675.

1282 Hanor, J. S. 1978. Precipitation of beachrock cements: mixing of marine and meteoric waters vs. CO^2-
1283 degassing. Journal of Sedimentary Research 48, 489-501.

1284 Herak, M., Herak, D., Markušić, S. 1996. Revision of the earthquake catalogue and seismicity of Croatia,
1285 1908–1992. Terra Nova 8(1), 86-94.

1286 Higginbotham, J. A. 1997. Piscinae: artificial fishponds in Roman Italy. UNC Press Books.

1287 Hijma, M., Engelhart, S.E., Tornqvist, T.E., Horton, B.P., Hu, P., Hill, D., 2015. A protocol for a geological
1288 sea-level database. In: Shennan, I., Long, A., Horton, B.P. (Eds.), Handbook of Sea Level Research. Wiley,
1289 pp. 536-553.

1290 Hill, D.F., Griffiths, S.D., Peltier, W.R., Horton, B.P., Törnqvist, T.E. 2011. High-resolution numerical
1291 modeling of tides in the western Atlantic, Gulf of Mexico, and Caribbean Sea during the Holocene. Journal
1292 of Geophysical Research: Oceans (1978–2012) 116(C10).

1293 Hopley, D., 1986. Beachrock as a sea-level indicator. In: Van de Plassche O. (Ed.), Sea-level Research: A
1294 Manual for the Collection and Evaluation of Data, Geo Books, Norwich, pp. 157–173.

1295 Horton, B. P., Rahmstorf, S., Engelhart, S. E., Kemp, A. C. 2014. Expert assessment of sea-level rise by AD
1296 2100 and AD 2300. Quaternary Science Reviews 84, 1-6.

1297 Horton, B. P., Shennan, I. 2009. Compaction of Holocene strata and the implications for relative sea level
1298 change on the east coast of England. Geology 37(12), 1083-1086.

1299 Jedoui, Y., Kallel, N., Fontugne, M., Ismail, H. B., M'Rabet, A., Montacer, M. 1998. A high relative sea-
1300 level stand in the middle Holocene of southeastern Tunisia. Marine Geology 147(1), 123-130.

1301 Jolivet, L., Augier, R., Faccenna, C., Negro, F., Rimmele, G., Agard, P., Robin, C., Rossetti, F., Crespo-
1302 Blanc, A. 2008. Subduction, convergence and the mode of backarc extension in the Mediterranean region.
1303 Bulletin de la Société Géologique de France 179(6), 525-550.

1304 Jolivet, L., Faccenna, C. 2000. Mediterranean extension and the Africa-Eurasia collision. Tectonics, 19(6),
1305 1095-1106.

1306 Juggins, S., Birks, H.J.B. 2012. Quantiative environmental reconstructions from biological data. In: Birks,
1307 H.J.B., Lotter, A.F., Juggins, S., Smol, J.P. (Eds). Data Handling and Numerical Techniques. Springer, pp.
1308 431-494.

1309 Khan, N. S., Ashe, E., Shaw, T. A., Vacchi, M., Walker, J., Peltier, W. R., Kopp, R.E., Horton, B. P. 2015.
1310 Holocene Relative Sea-Level Changes from Near-, Intermediate-, and Far-Field Locations. Current Climate
1311 Change Reports 1(4), 247-262.

1312 Kelletat, D. 2006. Beachrock as sea-level indicator? Remarks from a geomorphological point of view.
1313 Journal of Coastal Research, 1558-1564.

1314 Kemp, A. C., Horton, B. P., Donnelly, J. P., Mann, M. E., Vermeer, M., Rahmstorf, S. 2011. Climate related
1315 sea-level variations over the past two millennia. Proceedings of the National Academy of Sciences 108(27),
1316 11017–11022.

1317 Kemp, A. C., Telford, R.J. 2015. Transfer functions. In: Shennan, I., Long, A., Horton, B.P. (Eds.),
1318 Handbook of Sea Level Research. Wiley, pp. 470-499.

1319 Kopp, R. E., Simons, F. J., Mitrovica, J. X., Maloof, A. C., Oppenheimer, M. 2009. Probabilistic assessment
1320 of sea level during the last interglacial stage. Nature 462(7275), 863-867.

1321 Kjerfve, B. 1994. Coastal lagoons. Elsevier oceanography series 60, 1-8.

1322 Laborel, J., Laborel-Deguen, F. 1994. Biological indicators of relative sea-level variations and of co-seismic
1323 displacements in the Mediterranean region. Journal of Coastal Research 395-415.

1324 Laborel, J., Morhange, C., Lafont, R., Le Campion, J., Laborel-Deguen, F., Sartoretto, S. 1994. Biological
1325 evidence of sea-level rise during the last 4500 years on the rocky coasts of continental southwestern France
1326 and Corsica. Marine Geology 120(3), 203-223.

1327 Lachenal, A.-M., 1989. Écologie des ostracodes du domaine méditerranéen : application au Golfe de Gabès
1328 (Tunisie orientale). Les variations du niveau marin depuis 30,000 ans. Documents des laboratoires de
1329 géologie de Lyon 108, 1-239.

1330 Lakhdar, R., Soussi, M., Ben Ismail, M. H., M'Rabet, A. 2006. A Mediterranean Holocene restricted coastal
1331 lagoon under arid climate: Case of the sedimentary record of Sabkha Boujmel (SE Tunisia).
1332 Palaeogeography, Palaeoclimatology, Palaeoecology 241(2), 177-191.

1333 Lambeck, K., Antonioli, F., Anzidei, M., Ferranti, L., Leoni, G., Scicchitano, G., Silenzi, S. 2011. Sea level
1334 change along the Italian coast during the Holocene and projections for the future. Quaternary International
1335 232(1), 250-257.

1336 Lambeck, K., Antonioli, F., Purcell, A., Silenzi, S. 2004a. Sea-level change along the Italian coast for the
1337 past 10,000 yr. Quaternary Science Reviews 23(14), 1567-1598.

1338 Lambeck, K., Anzidei, M., Antonioli, F., Benini, A., Esposito, A. 2004b. Sea level in Roman time in the
1339 Central Mediterranean and implications for recent change. Earth and Planetary Science Letters 224(3), 563-
1340 575.

1341 Lambeck, K., Bard, E. 2000. Sea-level change along the French Mediterranean coast for the past 30 000
1342 years. Earth and Planetary Science Letters 175(3), 203-222.

1343 Lambeck, K., Purcell, A. 2005. Sea-level change in the Mediterranean Sea since the LGM: model
1344 predictions for tectonically stable areas. Quaternary Science Reviews 24(18), 1969-1988.

1345 Lambeck, K., Rouby, H., Purcell, A., Sun, Y., Sambridge, M. 2014. Sea level and global ice volumes from
1346 the Last Glacial Maximum to the Holocene. Proceedings of the National Academy of Sciences 111(43),
1347 15296-15303.

1348 Marco-Barba, J., Holmes, J. A., Mesquita-Joanes, F., Miracle, M. R. 2013. The influence of climate and
1349 sea-level change on the Holocene evolution of a Mediterranean coastal lagoon: Evidence from ostracod
1350 palaeoecology and geochemistry. Geobios 46(5), 409-421.

1351 Marcos, M., Tsimplis, M. N., Shaw, A. G. 2009. Sea level extremes in southern Europe. Journal of
1352 Geophysical Research: Oceans (1978–2012), 114(C1).

1353 Marra, F., Bozzano, F., Cinti, F. R. 2013. Chronostratigraphic and lithologic features of the Tiber River
1354 sediments (Rome, Italy): Implications on the post-glacial sea-level rise and Holocene climate. Global and
1355 Planetary Change 107, 157-176.

1356 Marriner, N., Flaux, C., Morhange, C., Kaniewski, D. 2012a. Nile Delta's sinking past: Quantifiable links
1357 with Holocene compaction and climate-driven changes in sediment supply? Geology 40(12), 1083-1086.

1358 Marriner, N., Gambin, T., Djamali, M., Morhange, C., Spiteri, M. 2012b. Geoarchaeology of the Burmarrad
1359 ria and early Holocene human impacts in western Malta. Palaeogeography, Palaeoclimatology,
1360 Palaeoecology 339, 52-65.

1361 Marriner, N., Morhange, C. 2007. Geoscience of ancient Mediterranean harbours. Earth-Science Reviews
1362 80(3), 137-194.

1363 Marriner, N., Morhange, C., Faivre, S., Flaux, C., Vacchi, M., Miko, S., Rossi, I. R. 2014. Post-Roman sea-
1364 level changes on Pag Island (Adriatic Sea): Dating Croatia's "enigmatic" coastal notch? Geomorphology
1365 221, 83-94.

1366 Maselli, V., Trincardi, F. 2013. Man made deltas. Scientific reports 3.

1367 Mastronuzzi, G., Sansò, P. 2012. The role of strong earthquakes and tsunami in the Late Holocene evolution
1368 of the Fortore River coastal plain (Apulia, Italy): A synthesis. Geomorphology 138(1), 89-99.

1369 Mastronuzzi, G., Sanso, P. 2002. Holocene uplift rates and historical rapid sea-level changes at the Gargano
1370 promontory, Italy. Journal of Quaternary Science 17(5-6), 593-606.

1371 Mauz, B., Ruggieri, G., Spada, G. 2015a. Terminal Antarctic melting inferred from a far-field coastal site.
1372 Quaternary Science Reviews 116, 122-132.

1373 Mauz, B., Vacchi, M., Green, A., Hoffmann, G., Cooper, A. 2015b. Beachrock: A tool for reconstructing
1374 relative sea level in the far-field. Marine Geology 362, 1-16.

1375 Mazzini, I., Anadon, P., Barbieri, M., Castorina, F., Ferreli, L., Gliozzi, E., Mola, M., Vittori, E. 1999. Late
1376 Quaternary sea-level changes along the Tyrrhenian coast near Orbetello (Tuscany, central Italy):
1377 palaeoenvironmental reconstruction using ostracods. Marine Micropaleontology 37(3), 289-311.

1378 McClennen, C.E., Housley, R.A. 2006. Late-Holocene channel meander migration and mudflat accumulation
1379 rates, lagoon of Venice, Italy. Journal of Coastal Research 930-945.

1380 Micallef, A., Foglini, F., Le Bas, T., Angeletti, L., Maselli, V., Pasuto, A., Taviani, M. (2013). The
1381 submerged paleolandscape of the Maltese Islands: Morphology, evolution and relation to Quaternary
1382 environmental change. Marine Geology 335, 129-147.

1383 Milli, S., D'Ambrogi, C., Bellotti, P., Calderoni, G., Carboni, M. G., Celant, A., Di Bella, L., Di Rita, F.,
1384 Frezza, V., Magri, D., Pichezzi R.M., Ricci, V. 2013. The transition from wave-dominated estuary to wave-
1385 dominated delta: the Late Quaternary stratigraphic architecture of Tiber River deltaic succession (Italy).
1386 Sedimentary Geology 284, 159-180.

1387 Milne, G.A., Long, A.J., Bassett, S.E., 2005. Modeling Holocene relative sea-level observations from the
1388 Caribbean and South America. Quaternary Science Reviews 24, 1183-1202.

1389 Milne, G. A., Mitrovica, J. X. 1998. Postglacial sea-level change on a rotating Earth. Geophysical Journal
1390 International 133(1), 1-19.

1391 Milne, G. A., Mitrovica, J. X. 2008. Searching for eustasy in deglacial sea-level histories. Quaternary
1392 Science Reviews, 27(25), 2292-2302.

1393 Mitrovica, J. X., Milne, G. A. 2002. On the origin of late Holocene sea-level highstands within equatorial
1394 ocean basins. Quaternary Science Reviews 21(20), 2179-2190.

1395 Morhange C., Marriner N., 2015. Archaeological and biological relative sea-level indicators. In: Shennan, I.,
1396 Long, A., Horton, B.P. (Eds.), Handbook of Sea Level Research. Wiley,, Wiley, pp. 146-156.

1397 Morhange, C., Laborel, J., Hesnard, A. 2001. Changes of relative sea level during the past 5000 years in the
1398 ancient habour of Marseilles, Southern France. Palaeogeography, Palaeoclimatology, Palaeoecology 166(3),
1399 319-329.

1400 Morhange, C., Marriner, N., Excoffon, P., Bonnet, S., Flaux, C., Zibrowius, H., Goiran, J. Amouri, M. E.
1401 2013. Relative Sea-Level Changes During Roman Times in the Northwest Mediterranean: The 1st Century
1402 AD Fish Tank of Forum Julii, Fréjus, France. Geoarchaeology 28(4), 363-372.

1403 Morhange, C., Marriner, N., Laborel, J., Todesco, M., Oberlin, C. 2006. Rapid sea-level movements and
1404 noneruptive crustal deformations in the Phlegrean Fields caldera, Italy. Geology 34(2), 93-96.

1405 Morhange, C., Pirazzoli, P. A. 2005. Mid-Holocene emergence of southern Tunisian coasts. Marine Geology
1406 220(1), 205-213.

1407 Morri, C., Bellan-Santini, D., Giaccone, G., Bianchi, C. N. 2004. Principles of bionomy: definition of
1408 assemblages and use of taxonomic descriptors (macrobenthos). Biologia Marina Mediterranea 11(1), 573-
1409 600.

1410 Nachite, D., Rodríguez-Lázaro, J., Martín-Rubio, M., Pascual, A., Bekkali, R. 2010. Distribution et écologie
1411 des associations d'ostracodes récents de l'estuaire de Tahadart (Maroc Nord-Occidental). Revue de
1412 micropaléontologie 53(1), 3-15.

1413 Nelson, A.R., Shennan, I., Long A. J., 1996. Identifying coseismic subsidence in tidal-wetland stratigraphic
1414 sequences at the Cascadia subduction zone of western North America, Journal of Geophysical Research 101,
1415 6115-6135.

1416 Nesteroff, W. D. 1984. Étude de quelques grès de plage du sud de la Corse: datations ^{14}C et implications
1417 néotectoniques pour le bloc corso-sarde. Travaux de la Maison de l'Orient 8(1), 99-111.

1418 Neumeier, U. 1998. The role of microbial activity in early cementation of beachrocks (intertidal sediments).
1419 Unpublished PhD thesis, University of Geneva.

1420 Nikula, R., Väinölä, R. 2003. Phylogeography of *Cerastoderma glaucum* (Bivalvia: Cardiidae) across
1421 Europe: a major break in the Eastern Mediterranean. Marine Biology 143(2), 339-350.

1422 Olivera, C., Susagna, T., Roca, A., Goula, X. 1992. Seismicity of the Valencia trough and surrounding areas.
1423 Tectonophysics 203(1), 99-109.

1424 Orrù, P. E., Antonioli, F., Lambeck, K., Verrubbi, V. 2004. Holocene sea-level change in the Cagliari coastal
1425 plain (southern Sardinia, Italy). Quaternaria Nova, 8, 193-212.

1426 Orrù, P. E., Mastronuzzi, G., Deiana, G., Pignatelli, C., Piscitelli, A., Solinas, E., Spanu, P., Zucca, R. 2014.
1427 Sea level changes and geoarchaeology between the bay of Capo Malfatano and Piscinnì Bay (SW Sardinia)
1428 in the last 4 kys. Quaternary International 336, 180-189.

1429 Orrù, P., Solinas, E., Puliga, G., Deiana, G. 2011. Palaeo-shorelines of the historic period, Sant'Antioco
1430 Island, south-western Sardinia (Italy). Quaternary International 232(1), 71-81.

1431 Parnell, A. C., Buck, C. E., Doan, T. K. 2011. A review of statistical chronology models for high-resolution,
1432 proxy-based Holocene palaeoenvironmental reconstruction. Quaternary Science Reviews 30(21), 2948-2960.

1433 Parnell, A.C., Gehrels, W.R. 2015. Using chronological models in late Holocene sea-level reconstructions
1434 from saltmarsh sediments. . In Handbook of Sea Level Research, Shennan I., Long A. J., Dr Benjamin P.
1435 Horton B. P. (Eds.). Wiley, pp 500-513.

1436 Pedley, M. 2011. The Calabrian Stage, Pleistocene highstand in Malta: a new marker for unravelling the Late
1437 Neogene and Quaternary history of the islands. Journal of the Geological Society 168(4), 913-926.

1438 Pedoja, K., Husson, L., Johnson, M.E., Melnick, D., Witt, C., Pochat, S., Nexer, M., Delcaillau, B., Pinegina,
1439 T., Poprawski, Y., Authemayou, C., Elliot, M., Regard, V., Garestier, F., 2014. Coastal staircase sequences
1440 reflecting sea-level oscillations and tectonic uplift during the Quaternary and Neogene. Earth-Science Rev.
1441 132, 13–38.

1442 Peltier, W. R., Fairbanks, R. G. 2006. Global glacial ice volume and Last Glacial Maximum duration from
1443 an extended Barbados sea level record. Quaternary Science Reviews 25(23), 3322-3337.

1444 Peltier, W. R., Tushingham, A. M. 1991. Influence of glacial isostatic adjustment on tide gauge
1445 measurements of secular sea level change. Journal of Geophysical Research: Solid Earth (1978–2012)
1446 96(B4), 6779-6796.

1447 Peltier, W.R., 2004. Global glacial isostasy and the surface of the ice-age earth: the ice-5G (VM2) model and
1448 grace. Annual Review of Earth and Planetary Sciences 32, 111-149.

1449 Pérès, J.M., Picard, J. 1964. Nouveau manuel de bionomie benthique de la mer Méditerranée. Recherches et
1450 Travaux de la Station Maritime d'Endoume 31, 1-137.

1451 Pirazzoli, P. A. 1976. Sea level variations in the northwest Mediterranean during Roman times. Science
1452 194(4264), 519-521.

1453 Pirazzoli, P. A. 2005. A review of possible eustatic, isostatic and tectonic contributions in eight late-
1454 Holocene relative sea-level histories from the Mediterranean area. Quaternary Science Reviews 24(18),
1455 1989-2001.

Pirazzoli, P. A., Stiros, S. C., Arnold, M., Laborel, J., Laborel-Deguen, F., Papageorgiou, S. 1994. Episodic uplift deduced from Holocene shorelines in the Perachora Peninsula, Corinth area, Greece. Tectonophysics 229(3), 201-209.

Preuss, H., 1979. Progress in computer evaluation of sea level data within the IGCP Project no. 61, in Proc. 1978 International Symposium of coastal evolution in the Quaternary. pp. 104.134.

Primavera, M., Simone, O., Fiorentino, G., Caldara, M. 2011. The palaeoenvironmental study of the Alimini Piccolo lake enables a reconstruction of Holocene sea-level changes in southeast Italy. The Holocene 21(4), 553-563.

Raynal, O., Bouchette, F., Certain, R., Sabatier, P., Lofi, J., Seranne, M., Courp, T. 2010. Holocene evolution of a Languedocian lagoonal environment controlled by inherited coastal morphology (northern Gulf of Lions, France). Bulletin de la Societe Geologique de France 181(2), 211-224.

Reimer, P., Reimer, R., 2001. A marine reservoir correction database and on-line interface. Radiocarbon 43, 461-463.

Reimer, P.J., Bard, E., Bayliss, A., Beck, J.W., Blackwell, P.G., Bronk Ramsey, C.,Buck, C.E., Cheng, H., Edwards, R.L., Friedrich, M., Grootes, P.M., Guilderson, T.P., Haflidason, H., Hajdas, I., Hatta, C., Heaton, T.J., Hogg, A.G., Hughen, K.A., Kaiser, K.F., Kromer, B., Manning, S.W., Niu, M., Reimer, R.W., Richards, D.A.,Scott, E.M., Southon, J.R., Turney, C.S.M., van der Plicht, J., 2013. IntCal13 andMARINE13 radiocarbon age calibration curves 0-50000 years cal BP. Radiocarbon 55.http://dx.doi.org/10.2458/azu_js_rc.55.16947

Reineck, H. E., Singh, I.B. 1973. Depositional sedimentary environments. FAO publishing.

Rossi, V., Amorosi, A., Sarti, G., Potenza, M. 2011. Influence of inherited topography on the Holocene sedimentary evolution of coastal systems: an example from Arno coastal plain (Tuscany, Italy). Geomorphology 135(1), 117-128.

Rovere, A., Antonioli, F., Bianchi, C. N. 2015. Fixed biological indicators. In: Handbook of Sea Level Research, Shennan I., Long A. J., Horton B.P. (Eds.). Wiley, pp. 268-280.

Rovere, A., Parravicini, V., Vacchi, M., Montefalcone, M., Morri, C., Bianchi, C. N., Firpo, M. 2010. Geo-environmental cartography of the marine protected area “Isola di Bergeggi”(Liguria, NW Mediterranean Sea). Journal of Maps 6(1), 505-519.

Rovere, A., Vacchi, M., Firpo, M., Carobene, L. 2011. Underwater geomorphology of the rocky coastal tracts between Finale Ligure and Vado Ligure (western Liguria, NW Mediterranean Sea). Quaternary International 232(1), 187-200.

Ruiz, F., Abad, M., Bodergat, A. M., Carbonel, P., Rodríguez-Lázaro, J., Yasuhara, M. 2005. Marine and brackish-water ostracods as sentinels of anthropogenic impacts. Earth-Science Reviews 72(1), 89-111.

1489 Ruiz, F., Abad, M., Galán, E., González, I., Aguilá, I., Olías, M., Goméz Ariza, G.L., Cantano, M. 2006. The
1490 present environmental scenario of El Melah Lagoon (NE Tunisia) and its evolution to a future sabkha.
1491 Journal of African Earth Sciences 44(3), 289-302.

1492 Sabatier, P., Dezileau, L., Barbier, M., Raynal, O., Lofi, J., Briqueu, L., Condomines, M., Bouchette, F.,
1493 Certain, R., Van Grafenstein, U., Jorda, C., Blanchemanche, P. 2010. (South of France). Bulletin de la
1494 Societe Geologique de France 181(1), 27-36.

1495 Sacchi, M., Molisso, F., Pacifico, A., Vigliotti, M., Sabbarese, C., Ruberti, D. 2014. Late-Holocene to recent
1496 evolution of Lake Patria, South Italy: An example of a coastal lagoon within a Mediterranean delta system.
1497 Global and Planetary Change 117, 9-27.

1498 Sammari, C., Koutitonsky, V. G., Moussa, M. 2006. Sea level variability and tidal resonance in the Gulf of
1499 Gabes, Tunisia. Continental Shelf Research 26(3), 338-350.

1500 Sarti, G., Centineo, M.C., Calabrese, L., 2009. Carta Geologica d'Italia alla scala 1:50.000. Foglio 205,
1501 Comacchio. Note illustrative.
1502 http://www.isprambiente.gov.it/Media/carg/note_illustrative/205_Comacchio.pdf

1503 Sartoretto, S., Verlaque, M., Laborel, J. 1996. Age of settlement and accumulation rate of submarine
1504 “coralligène”(− 10 to− 60 m) of the northwestern Mediterranean Sea; relation to Holocene rise in sea level.
1505 Marine Geology 130(3), 317-331.

1506 Schembri, P. J., Deidun, A., Mallia, A., Mercieca, L. 2005. Rocky shore biotic assemblages of the Maltese
1507 Islands (Central Mediterranean): a conservation perspective. Journal of Coastal Research, 157-166.

1508 Schmiedt, G. 1972. Il livello antico del mar Tirreno.Testimonianze da resti archeologici, Florence: E.
1509 Olschki

1510 Scicchitano, G., Antonioli, F., Berlinghieri, E.F.C., Dutton, A., Monaco, C. 2008. Submerged archaeological
1511 sites along the Ionian coast of southeastern Sicily (Italy) and implications for the Holocene relative sea-level
1512 change. Quaternary Research 70(1), 26-39.

1513 Scicchitano, G., Monaco, C., Tortorici, L. 2007. Large boulder deposits by tsunami waves along the Ionian
1514 coast of south-eastern Sicily (Italy). Marine Geology 238(1), 75-91.

1515 Scicchitano, G., Spampinato, C. R., Ferranti, L., Antonioli, F., Monaco, C., Capano, M., Lubritto, C. 2011.
1516 Uplifted Holocene shorelines at Capo Milazzo (NE Sicily, Italy): evidence of co-seismic and steady-state
1517 deformation. Quaternary International 232(1), 201-213.

1518 Serandrei-Barbero, R., Albani, A., Donnici, S., Rizzetto, F. 2006. Past and recent sedimentation rates in the
1519 Lagoon of Venice (Northern Italy). Estuarine, Coastal and Shelf Science 69(1), 255-269.

1520 Serpelloni, E., Faccenna, C., Spada, G., Dong, D., Williams, S. D. 2013. Vertical GPS ground motion rates
1521 in the Euro-Mediterranean region: New evidence of velocity gradients at different spatial scales along the
1522 Nubia-Eurasia plate boundary. Journal of Geophysical Research: Solid Earth 118(11), 6003-6024.

1523 Shennan, I. 1986. Flandrian sea-level changes in the Fenland. II: Tendencies of sea-level movement,
1524 altitudinal changes, and local and regional factors. Journal of Quaternary Science 1(2), 155-179.

1525 Shennan, I., Horton, B., 2002. Holocene land- and sea-level changes in Great Britain. Journal of Quaternary
1526 Science 17, 511-526.

1527 Shennan, I., Long, A. J., Horton, B.P., 2015. Handbook of Sea-Level Research. John Wiley & Sons.

1528 Shennan, I., Milne, G., Bradley, S., 2012. Late Holocene vertical land motion and relative sea level changes:
1529 lessons from the British Isles. Journal of Quaternary Science 27 (1) 64-70

1530 Silvestri, S., Defina, A., Marani, M. 2005. Tidal regime, salinity and salt marsh plant zonation. Estuarine,
1531 Coastal and Shelf Science 62(1), 119-130.

1532 Somoza, L., Barnolas, A., Arasa, A., Maestro, A., Rees, J. G., Hernández-Molina, F. J. 1998. Architectural
1533 stacking patterns of the Ebro delta controlled by Holocene high-frequency eustatic fluctuations, delta-lobe
1534 switching and subsidence processes. Sedimentary Geology 117(1), 11-32.

1535 Spada, G., Stocchi, P. 2007. SELEN: A Fortran 90 program for solving the “sea-level equation”. Computers
1536 & Geosciences 33(4), 538-562.

1537 Spampinato, C. R., Costa, B., Di Stefano, A., Monaco, C., Scicchitano, G. 2011. The contribution of
1538 tectonics to relative sea-level change during the Holocene in coastal south-eastern Sicily: new data from
1539 boreholes. Quaternary International 232(1), 214-227.

1540 Spampinato, C.R., Scicchitano, G., Ferranti, L., Monaco, C. 2012. Raised Holocene paleo-shorelines along
1541 the Capo Schisò coast, Taormina: New evidence of recent co-seismic deformation in northeastern Sicily
1542 (Italy). Journal of Geodynamics 55, 18-31.

1543 Stiros, S.C., Pirazzoli, P. A. 2008. Direct determination of tidal levels for engineering applications based on
1544 biological observations. Coastal Engineering 55(6), 459-467.

1545 Stocchi, P., Colleoni, F., Spada, G. 2009. Bounds on the time–history and Holocene mass budget of
1546 Antarctica from sea–level records in SE Tunisia. Pure and applied geophysics 166(8-9), 1319-1341.

1547 Stocchi, P., Spada, G. 2009. Influence of glacial isostatic adjustment upon current sea level variations in the
1548 Mediterranean. Tectonophysics 474(1), 56-68.

1549 Strasser, A., Davaud, E., Jedoui, Y. 1989. Carbonate cements in Holocene beachrock: example from Bahiret
1550 et Biban, southeastern Tunisia. Sedimentary Geology 62(1), 89-100.

Stuiver, M., Polach, H.A., 1977. Reporting ^{14}C data. Radiocarbon 19, 355-363.

Tornqvist, T.E., Rosenheim, B.E., Hu, P., Fernandez, A.B., 2015. Radiocarbon dating and calibration. In: Shennan, I., Long, A.J., Horton, B.P. (Eds.), Handbook of Sea- level Research. Wiley, pp. 349-360.

Törnqvist, T.E., Wallace, D.J., Storms, J.E.A., Wallinga, J., Van Dam, R.L., Blaauw, M., Derksen, M.S., Klerks, C.J.W., Meijneken, C., Snijders, E.M.A., 2008. Mississippi Delta subsidence primarily caused by compaction of Holocene strata. Nature Geoscience 1, 173-176.

Tortorici, G., Bianca, M., de Guidi, G., Monaco, C., Tortorici, L. 2003. Fault activity and marine terracing in the Capo Vaticano area (southern Calabria) during the Middle-Late Quaternary. Quaternary International 101, 269-278.

Triantaphyllou, M. V., Tsourou, T., Koukousioura, O., Dermitzakis, M. D. 2005. Foraminiferal and ostracod ecological patterns in coastal environments of SE Andros Island (Middle Aegean Sea, Greece). Revue de micropaléontologie 48(4), 279-302.

Tsimplis, M. N., Proctor, R., Flather, R. A. 1995. A two-dimensional tidal model for the Mediterranean Sea. Journal of Geophysical Research: Oceans (1978–2012), 100(C8), 16223-16239.

Vacchi, M., Rovere, A., Chatzipetros, A., Zouros, N., Firpo, M. 2014. An updated database of Holocene relative sea level changes in NE Aegean Sea. Quaternary International 328, 301-310.

Vacchi, M., Rovere, A., Schiaffino, C. F., Ferrari, M. 2012a. Monitoring the effectiveness of re-establishing beaches artificially: methodological and practical insights into the use of video transects and SCUBA-operated coring devices. Underwater Technology 30(4), 201.

Vacchi, M., Rovere, A., Zouros, N., Desruelles, S., Caron, V., Firpo, M. 2012b. Spatial distribution of sea-level markers on Lesvos Island (NE Aegean Sea): evidence of differential relative sea-level changes and the neotectonic implications. Geomorphology 159, 50-62.

van de Plassche, O., 1982. Sea-level change and water-level movements in the Netherlands during the Holocene. Mededelingen Rijks Geologische Dienst 36, 1-93

Vella, C., Fleury, T. J., Raccasi, G., Provansal, M., Sabatier, F., Bourcier, M. 2005. Evolution of the Rhône delta plain in the Holocene. Marine Geology 222, 235-265.

Vella, C., Provansal, M. 2000. Relative sea-level rise and neotectonic events during the last 6500yr on the southern eastern Rhône delta, France. Marine Geology 170(1), 27-39.

Vött, A. 2007. Relative sea level changes and regional tectonic evolution of seven coastal areas in NW Greece since the mid-Holocene. Quaternary Science Reviews 26(7), 894-919.

Vousdoukas, M. I., Velegrakis, A. F., Plomaritis, T. A. 2007. Beachrock occurrence, characteristics, formation mechanisms and impacts. Earth-Science Reviews 85(1), 23-46.

1583 Zaîbi, C., Carbonel, P., Kamoun, F., Azri, C., Kharroubi, A., Kallel, N., Jedoui, Y., Montacer, M., Fontugne,
1584 M. 2011. Évolution du trait de côte à l'Holocène supérieur dans la Sebkha El-Guettiate de Skhira (Golfe de
1585 Gabès, Tunisie) à travers sa faune d'ostracodes et de foraminifères. Geobios 44(1), 101-115.

1586

1587

1588 Figures and Appendix captions

1589

1590 Figure 1. Spatial extent of the study area. Numbered rectangles denote the location of sea-level data for this
1591 paper, grouped into regions as explained in the text. GS is Gibraltar Strait, CO is Corsica, SA is Sardinia, SI
1592 is Sicily.

1593

1594 Figure 2. Tectonic framework of the western Mediterranean. Faults are modified after Faccenna et al.,
1595 (2014). Squares indicate the average elevation of MIS 5e shorelines (data from Ferranti et al., 2006; Pedoja
1596 et al., 2014). Dots denote the on-going GPS-derived vertical movements along the Mediterranean coast (data
1597 from Serpelloni et al., 2013). CO, Corsica; SA, Sardinia; SI, Sicily. Al, Alicante; Va, Gulf of Valencia; Ed,
1598 Ebro Delta; Ll, Llobregat Delta; Cc, Cap Creus; Ca, Cap d'Agde; Rh, Rhone Delta; Pc, Port Cros; Fj, Frejus;
1599 Ge, Genova; Sz, La Spezia; Vs, Versilia plain; Ar, Arno river; Pn, Pianosa Island; Cv, Civitavecchia, CV; Ti,
1600 Tiber Delta; Fo, Fondi plain; P, Pontine Archipelago; Vp, Volturno plain; Na, Naples volcanic district; Sp;
1601 Sele plain; Cv, Capo Vaticano; Ms, Messina Strait; Mt, Marettimo Island; Pl, Capo Gallo; Ma, Marsala
1602 sound; Ct, Catania; Sy, Syracuse; Mf, Monfalcone; Vl, Venice lagoon; Pd, Po Delta; Rp, Romagna coastal
1603 plain; Ps, Pescara; Sg, Sangro plain; Gp, Gargano promontory; Md, Gulf of Manfredonia.

1604

1605 Figure 3. Schematic diagram of the indicative meaning and theoretical examples of its application in
1606 reconstructing RSL from radiocarbon-dated fixed biological samples (A), lagoonal and marsh samples (B)
1607 and beachrocks samples (C). RWL is the Reference Water Level, e_{IR} is the indicative range, e_n represents the
1608 sum of the error associated with sea level research, HMC is High Magnesium Calcite; MSL is the modern
1609 Mean Sea Level.

1610

1611 Figure 4. Location of the example site in Burmarrad, Malta. Molluscan and ostracod assemblages of the core
1612 BM1 indicate that the dated charcoal was deposited in semi-enclosed lagoon facies. The sample, collected at
1613 -10.1 MSL yielded a radiocarbon age of 6500 ±30 years (7326-7471 ka BP 2σ). After correction for the
1614 indicative range, we produced an index point placing the RSL at -9.6 ± 0.55 (details in section 3.3).
1615
1616 Figure 5. A) Stacked histogram of intercalated, basal, fixed biological, beachrocks and archaeological index
1617 points. B) Total plots of the 473 index points used for the RSL reconstructions in the 22 regions. Index
1618 points are divided into intercalated, basal, fixed biological, beachrocks and archaeological indicators.
1619
1620 Figure 6. RSL reconstructions in central Spain (#1), northern Spain (#2) and central France (#3). Index
1621 points (boxes) are plotted as calibrated age against change in sea level relative to present. Limiting points are
1622 plotted as terrestrial or marine horizontal lines. Dimensions of boxes and lines for each point based on 2s
1623 elevation and age errors. The relative sea-level data is compared to a prediction (red line with minimum and
1624 maximum errors) from the SELEN model (see section 4). Al, Alicante; Va, Valencia. Ed, Ebro Delta; Cu,
1625 Cubelles; Ll, Llobregat Delta; Em, Empuries. Lg, Languedoc lagoons; Rh, Rhone Delta, Eb, Etang de Berre,
1626 Ma, Marseille; Lc, La Ciotat; Pc, Port Cros.
1627
1628 Figure 7. RSL reconstructions in RSL reconstructions in RSL reconstructions in RSL reconstructions in RSL
1629 reconstructions in Index points (boxes) are plotted as calibrated age against change in sea level relative to
1630 present. Limiting points are plotted as terrestrial or marine horizontal lines. The dimensions of boxes and
1631 lines for each point are based on 2s elevation and age errors. The relative sea-level data is compared to a
1632 prediction (red line with minimum and maximum errors) from the SELEN model (see section 4). Red dots
1633 denote the approximate location of the cluster of RSL data-points. Fj, Frejus; Ni, Nice coastal plain; Sv,
1634 Savona; Ge, Genova. Sp, La Spezia; Vs, Versilia coastal plain, Pi, Pisa; Ar, Arno coastal plain. Cc, Cap
1635 Corse; Sc, Scandola; Pn, Pianosa. Vl, Gulf of Valinco; Bs, Bonifacio Strait; Ol, Olbia; Cl, Cala Liberotto,
1636 Ca, Capo Caccia.
1637

1638 Figure 8: RSL reconstructions in southwestern Sardinia (#8), RSL reconstructions in southwestern Sardinia
1639 (#8), RSL reconstructions in southwestern Sardinia (#8), Index points (boxes) are plotted as calibrated age
1640 against change in sea level relative to present. Limiting points are plotted as terrestrial or marine horizontal
1641 lines. Dimensions of boxes and lines for each point based on 2s elevation and age errors. The relative sea-
1642 level data are compared to a prediction (red line with minimum and maximum errors) from the SELEN
1643 model (see section 4). Red dots represent the approximate location of RSL data-points. Th, Tharros, Mi, Is
1644 Mistras, Or, Gulf of Oristano, Pi, Piscinni Bay and Malfatano Cape; St, Sant'Antioco; Ca, Cagliari; No,
1645 Nora. Cv, Civitavecchia; Sm, Santa Marinella, Ti, Tiber Delta. Fo, Fondi coastal plain; Fr, Formia; Po,
1646 Pontine Archipelago; Vp, Volturno coastal plain. Sp, Sele coastal plain.
1647
1648 Figure 9. RSL reconstructions in northwestern Sicily (#12), mid-eastern Sicily (#13), southeastern Sicily
1649 (#14) and southern Tunisia (#15). Index points (boxes) are plotted as calibrated age against change in sea
1650 level relative to present. Limiting points are plotted as terrestrial or marine horizontal lines. Dimensions of
1651 boxes and lines for each point based on 2s elevation and age errors. The relative sea level data is compared
1652 to a prediction (red line with minimum and maximum errors) from the SELEN model (see section 4). Red
1653 dots denote the location of RSL data-points. Mt, Marettimo; Ma, Marsala sound; Sv, Cape San Vito; Pl,
1654 Palermo. Ca, Catania coastal plain; Au, Augusta; Sy, Syracuse. Av, Avola; Pa, Pachino; Br, Bourammad,
1655 Ms, Marsaxlokk. Dj, Djerba Island; Gu, Gulf of Gabes.
1656
1657 Figure 10. RSL reconstructions in Venice and Friuli lagoons (#16), northeastern Adriatic Sea (#17), and
1658 northwestern Adriatic Sea (#18). Index points (boxes) are plotted as calibrated age against change in sea
1659 level relative to present. Limiting points are plotted as terrestrial or marine horizontal lines. Dimensions of
1660 boxes and lines for each point based on 2s elevation and age errors. The relative sea-level data are compared
1661 to a prediction (red line with minimum and maximum errors) from the SELEN model (see section 4). Red
1662 dots represent the approximate location of RSL data-points. Vl, Venice lagoon; Cl, Caorle lagoon; Gl, Grado
1663 lagoon; Mf, Monfalcone. Tr, Gulf of Trieste, Pg, Pag Island. Pd, Po Delta; Cm, Comacchio coastal plain; Rp,
1664 Romagna coastal plain.
1665

1666 Figure 11. RSL history in mid-eastern Adriatic Sea (#19), mid-western Adriatic Sea (#20), northern Apulia
1667 (#21) and southern Apulia (#22). Index points (boxes) are plotted as calibrated age against change in sea
1668 level relative to present. Limiting points are plotted as terrestrial or marine horizontal lines. Dimensions of
1669 boxes and lines for each point based on 2s elevation and age errors. The relative sea-level data are compared
1670 to a prediction (red line with minimum and maximum errors) from the SELEN model (see section 4). Red
1671 dots represent the approximate location of RSL data-points. Vi, Vis Island; Bs, Bisevo Island. Ps, Pescara
1672 coastal plain; Sg, Sangro coastal plain; Bt, Battaglia lake; Mf, Gulf of Manfredonia; Fr, Frattarolo lagoon.
1673 Eg, Egnazia; Al, Alimini piccolo lake.
1674
1675 Figure 12. Example of the applicability of the proposed multiproxy standardization in central France (A),
1676 southern Tunisia (B), and southwestern Sardinia (C). Index points (boxes) are plotted as calibrated age
1677 against change in sea level relative to present. Limiting points are plotted as terrestrial or marine horizontal
1678 lines. The dimensions of boxes and lines for each point are based on 2s elevation and age errors.
1679
1680 Figure 13. A) Total plot of the western Mediterranean index points from areas that are tectonically stable and
1681 minimally affected by compaction-related subsidence. B) Variability of late Holocene (last 4.0 ka BP) RSL
1682 index points in the western Mediterranean. Note that the x and y axis are forced to the MSL at A.D. 1900. C)
1683 Approximate location of the index points plotted (red dots) and not plotted (grey dots) in panel a, see section
1684 6.3 for details. D) Normal distribution of late Holocene rising rates plotted against the 20^{th} century RSL rise
1685 (with error) derived from long-term Mediterranean tidal gauges (see table 3). Number above squares denotes
1686 the number of years used to compute the trend. MG, Malaga; MS, Marseille; GE, Genova; VE, Venezia P.
1687 Salute; TR, Trieste; RO, Rovinj; BK, Bakar; SP, Split Gradska; DB, Dubrovnik.
1688
1689 Appendix A. RSL database of the Western Mediterranean coast.
1690 Appendix B. Bibliography of the original sources used to compile the database in Appendix A.

Figure 1

Click here to download high resolution image

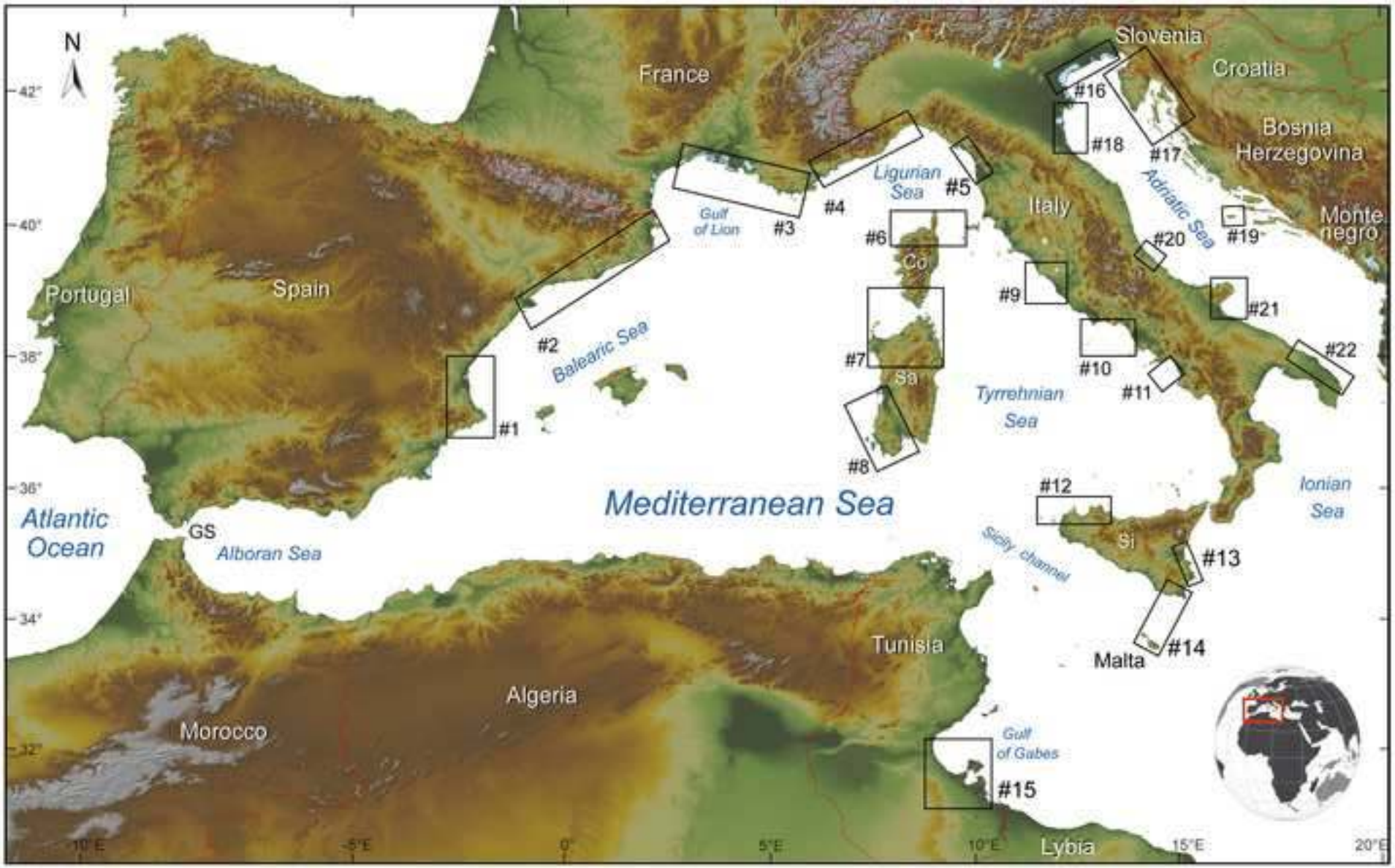

Figure 2

Click here to download high resolution image

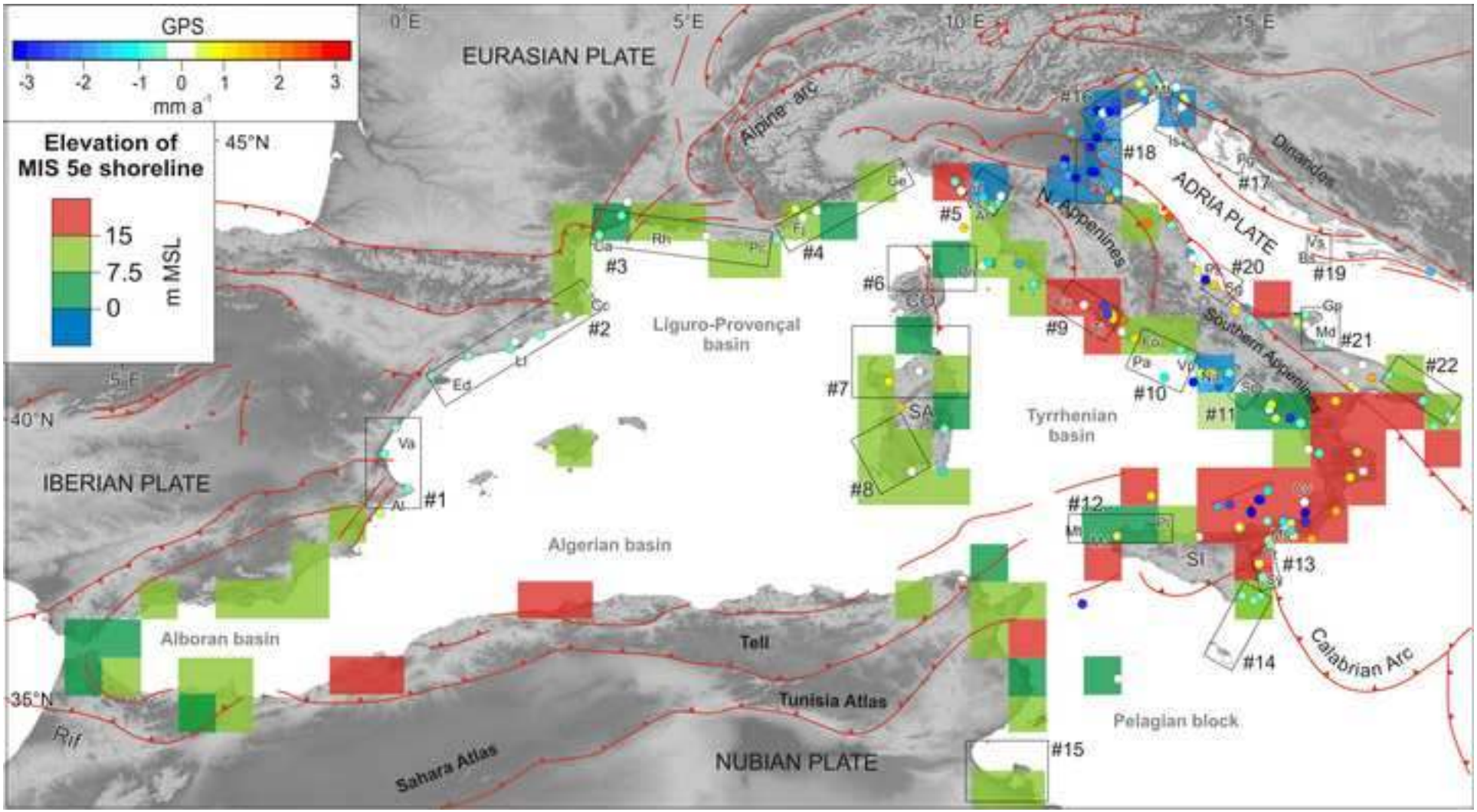

Figure

Click here to download high resolution image

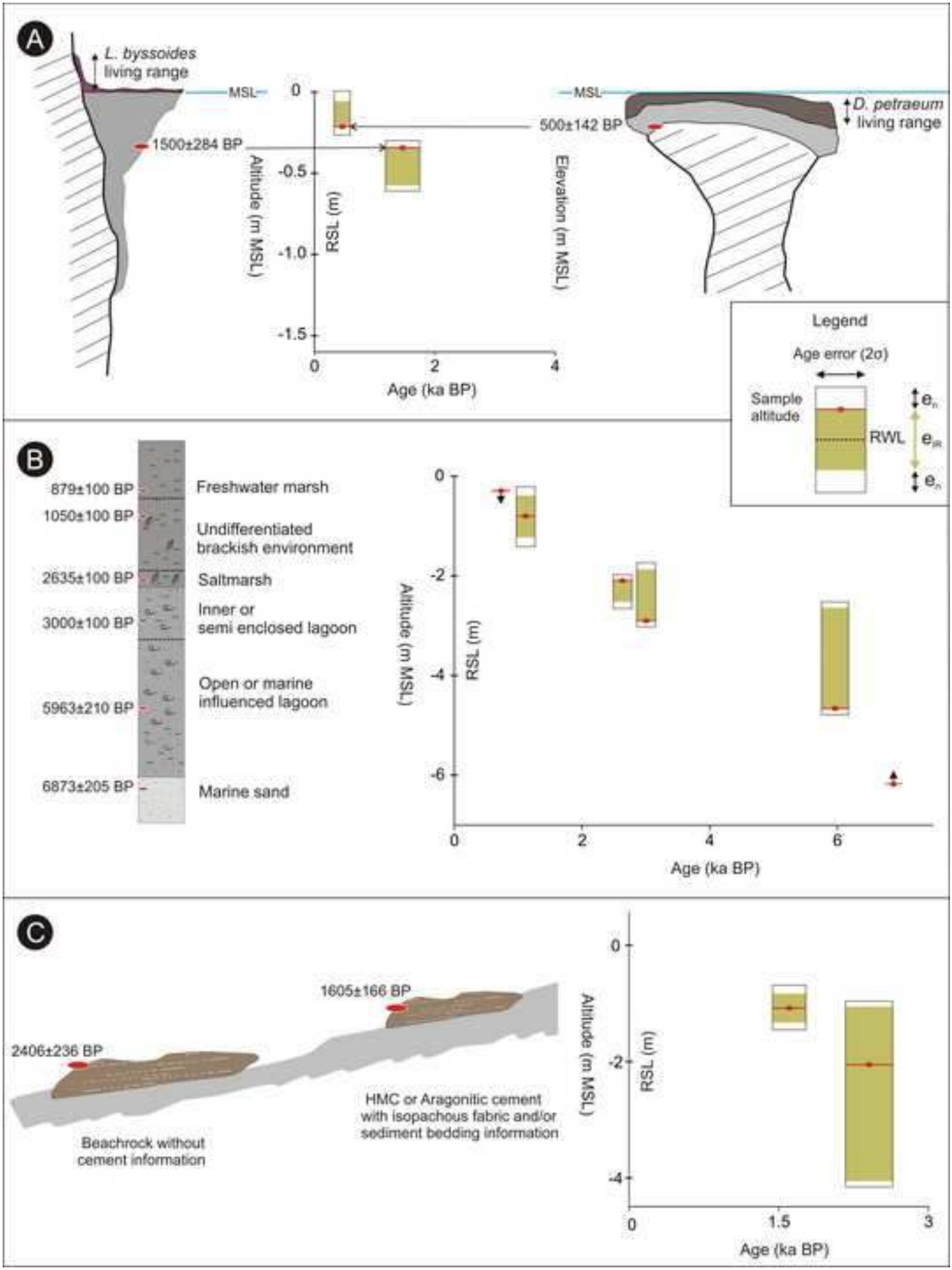

Figure 4

Click here to download high resolution image

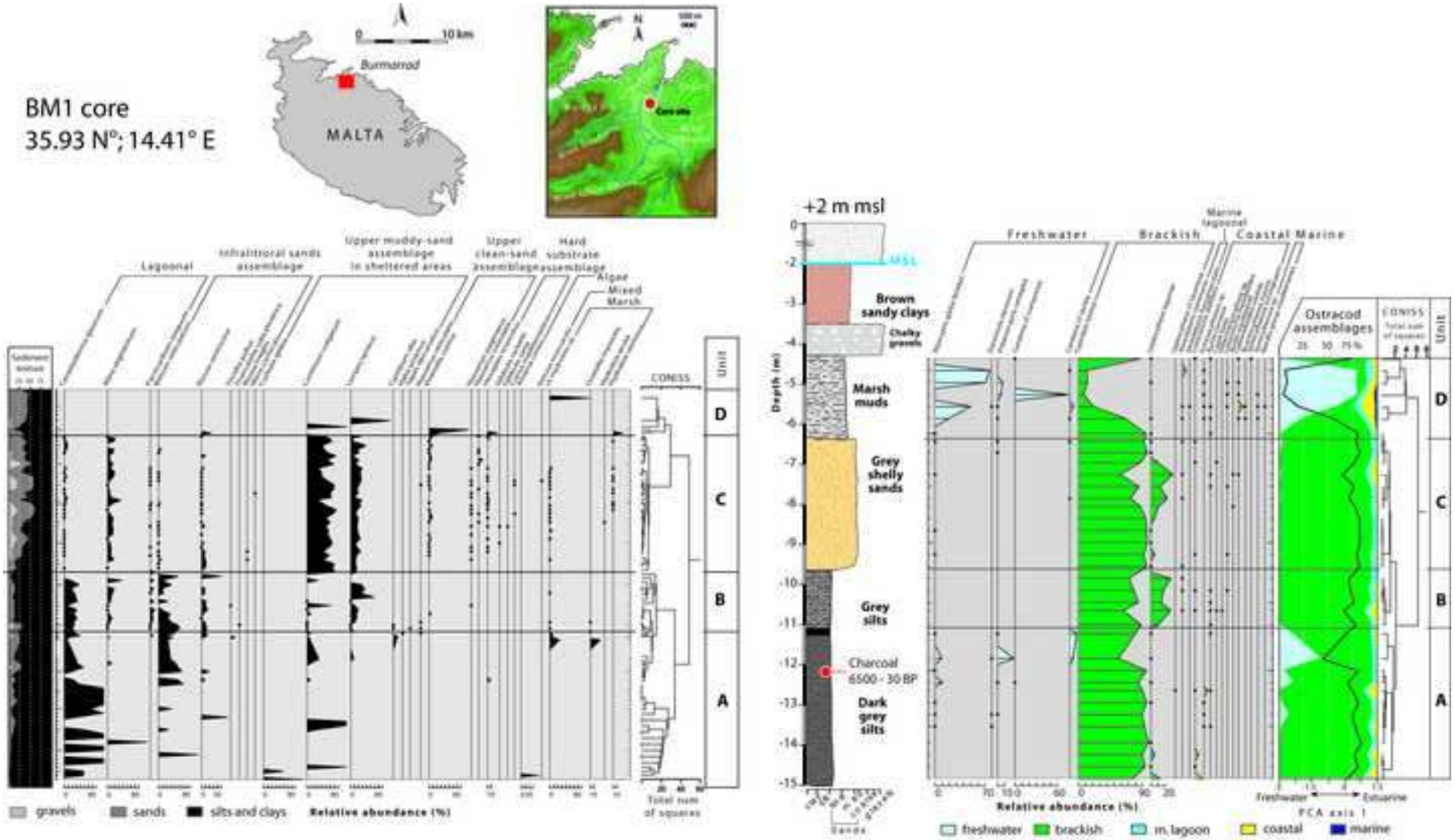

Figure 5

Click here to download high resolution image

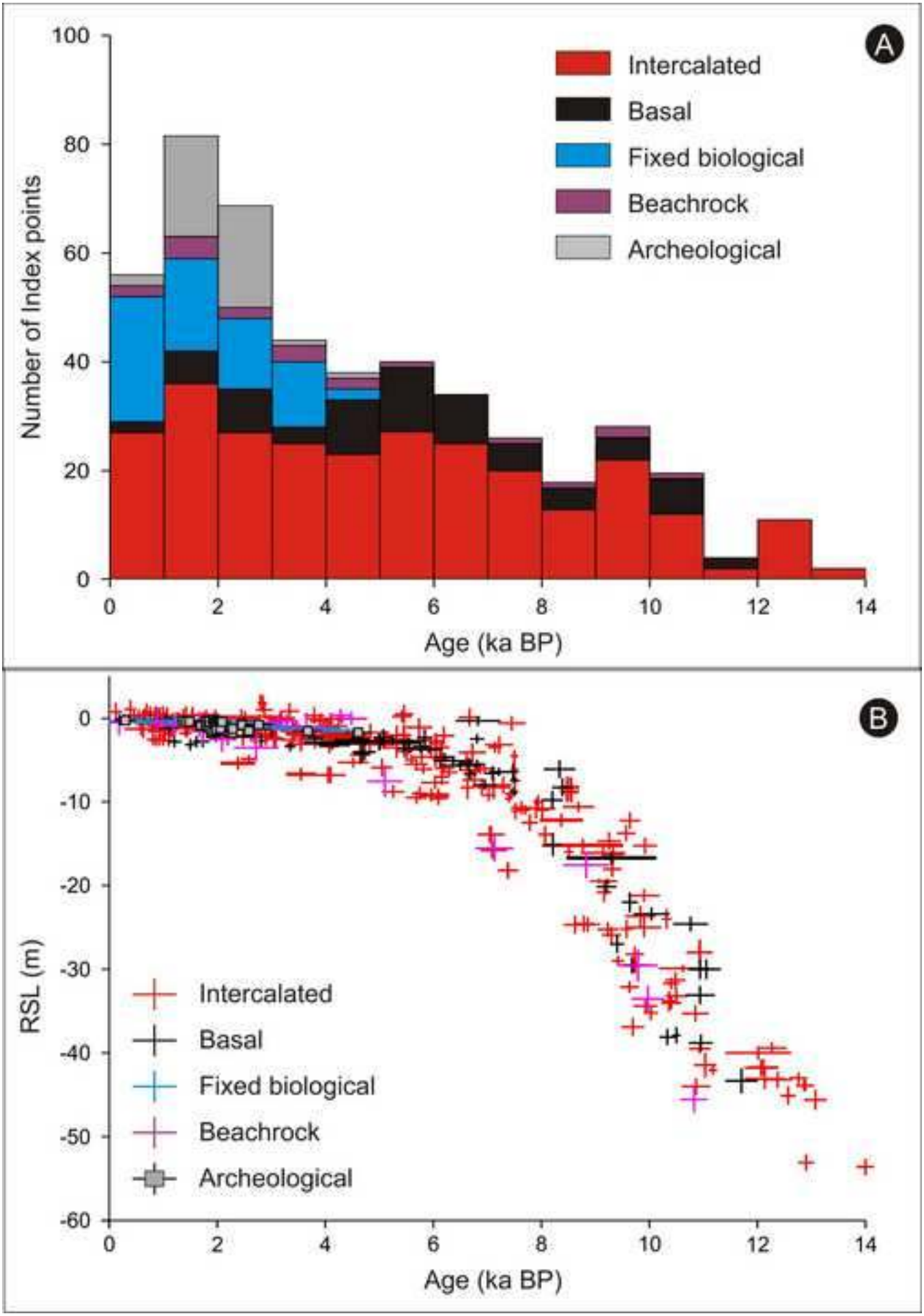

Figure 6

Click here to download high resolution image

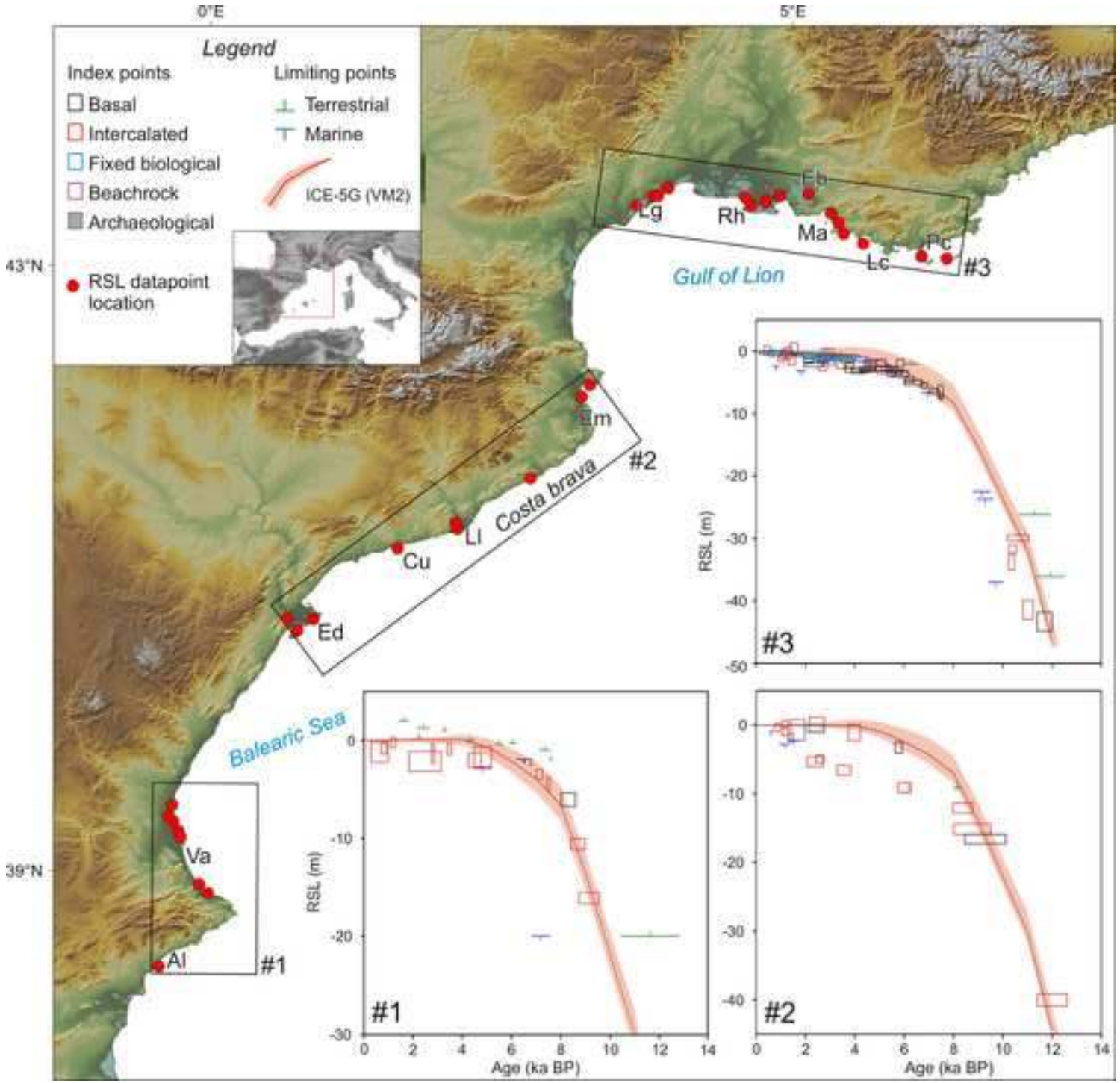

Figure 7

Click here to download high resolution image

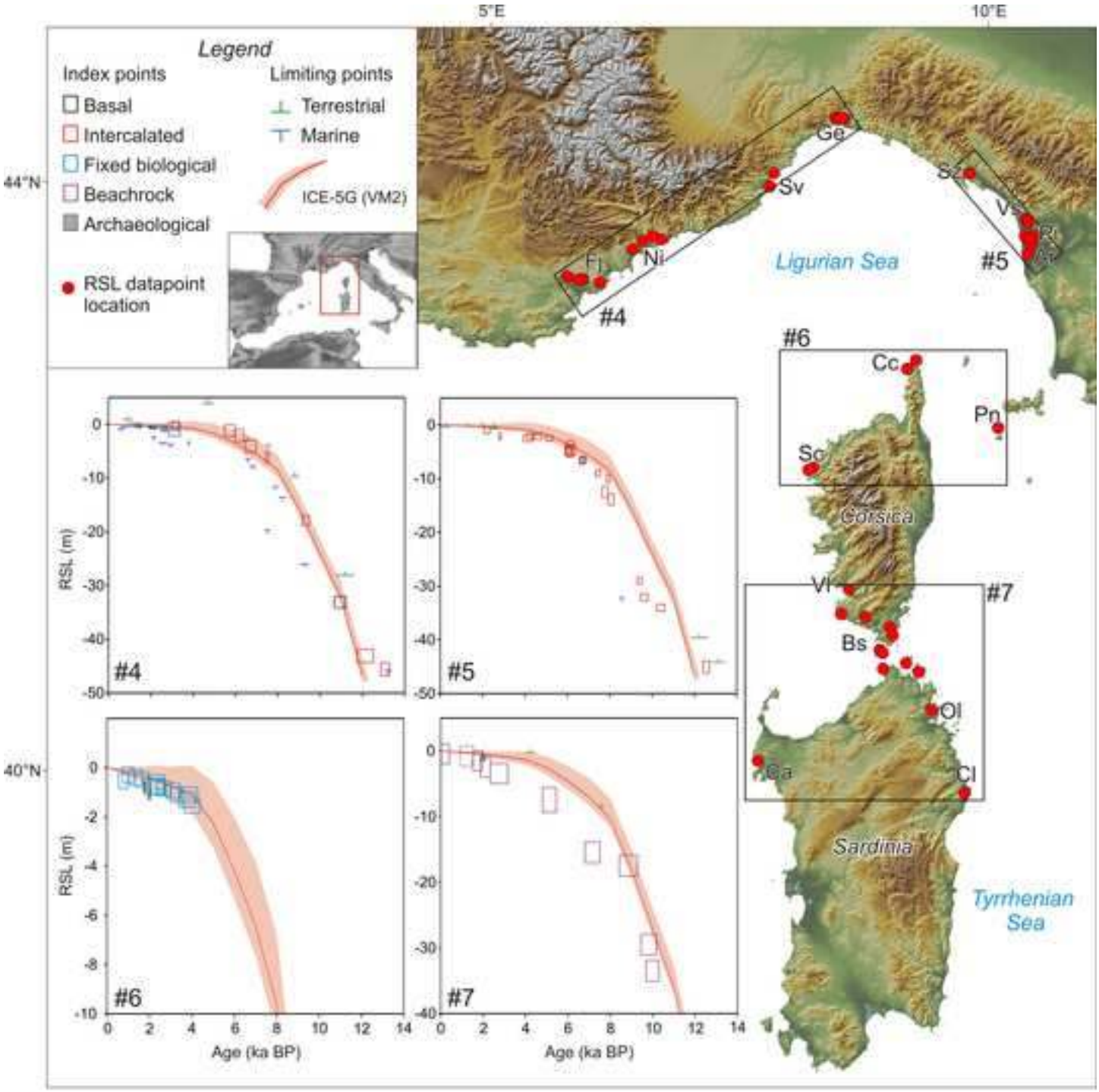

Figure 8

Click here to download high resolution image

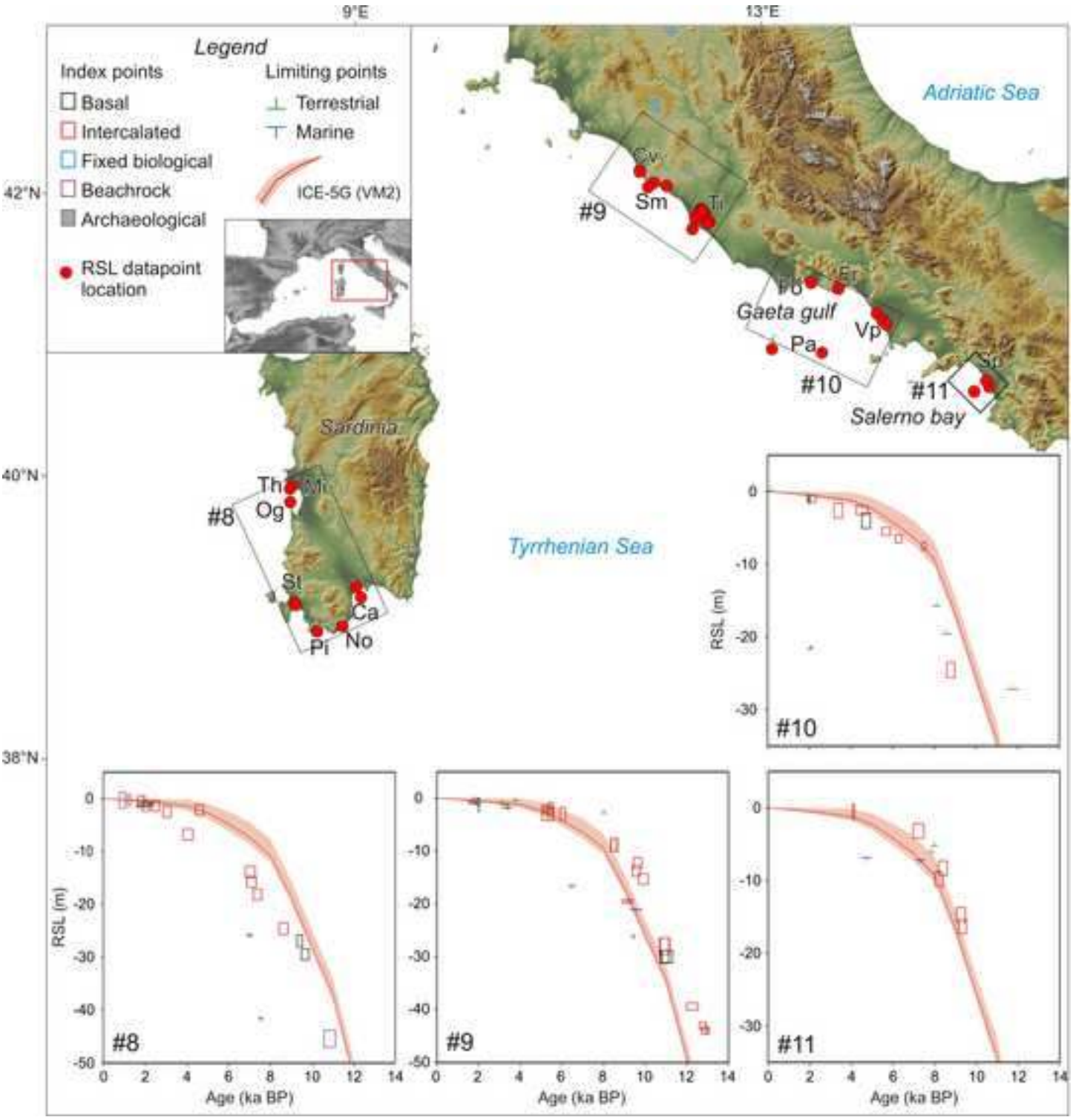

Figure 9

Click here to download high resolution image

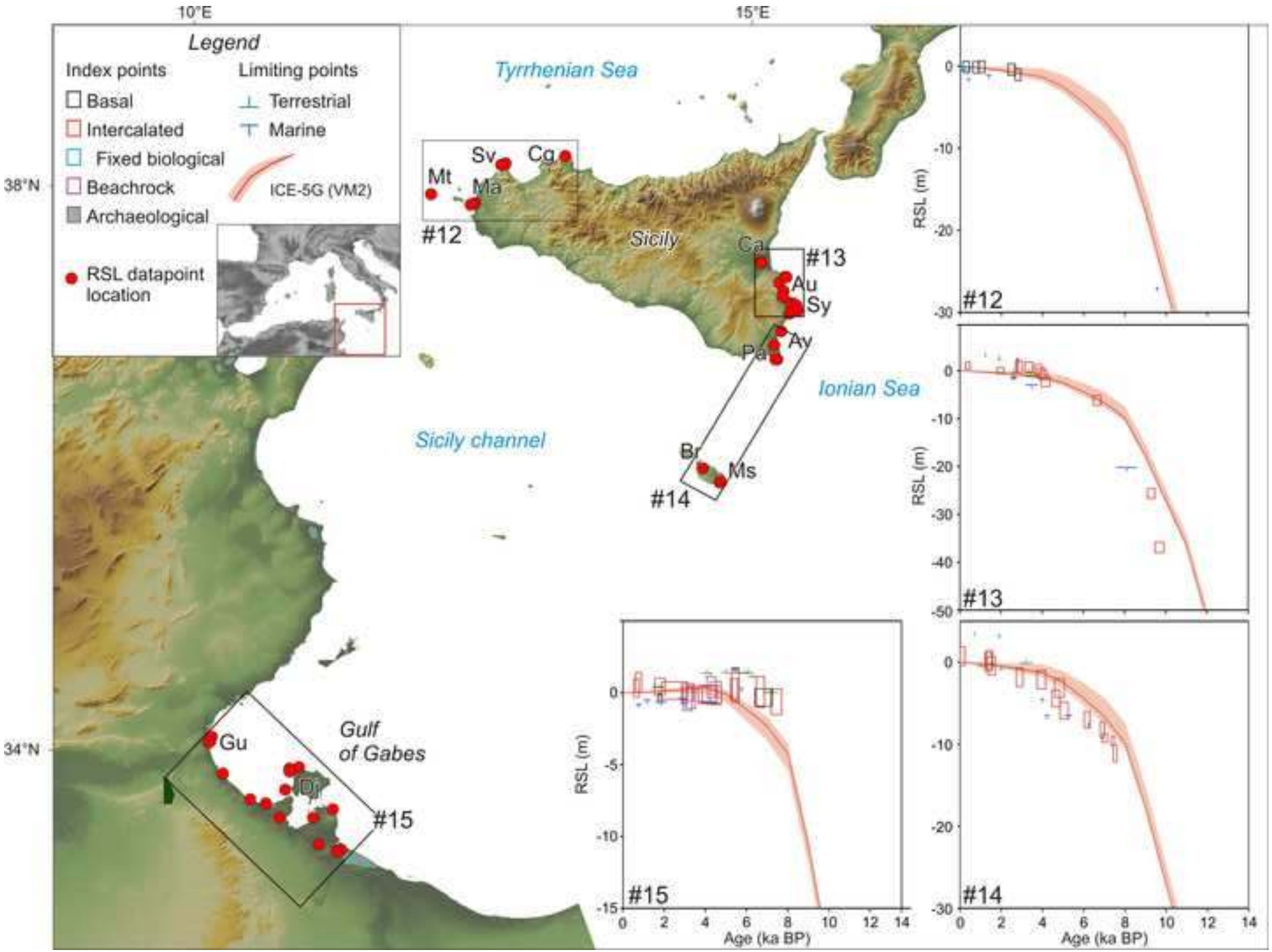

Figure 10

Click here to download high resolution image

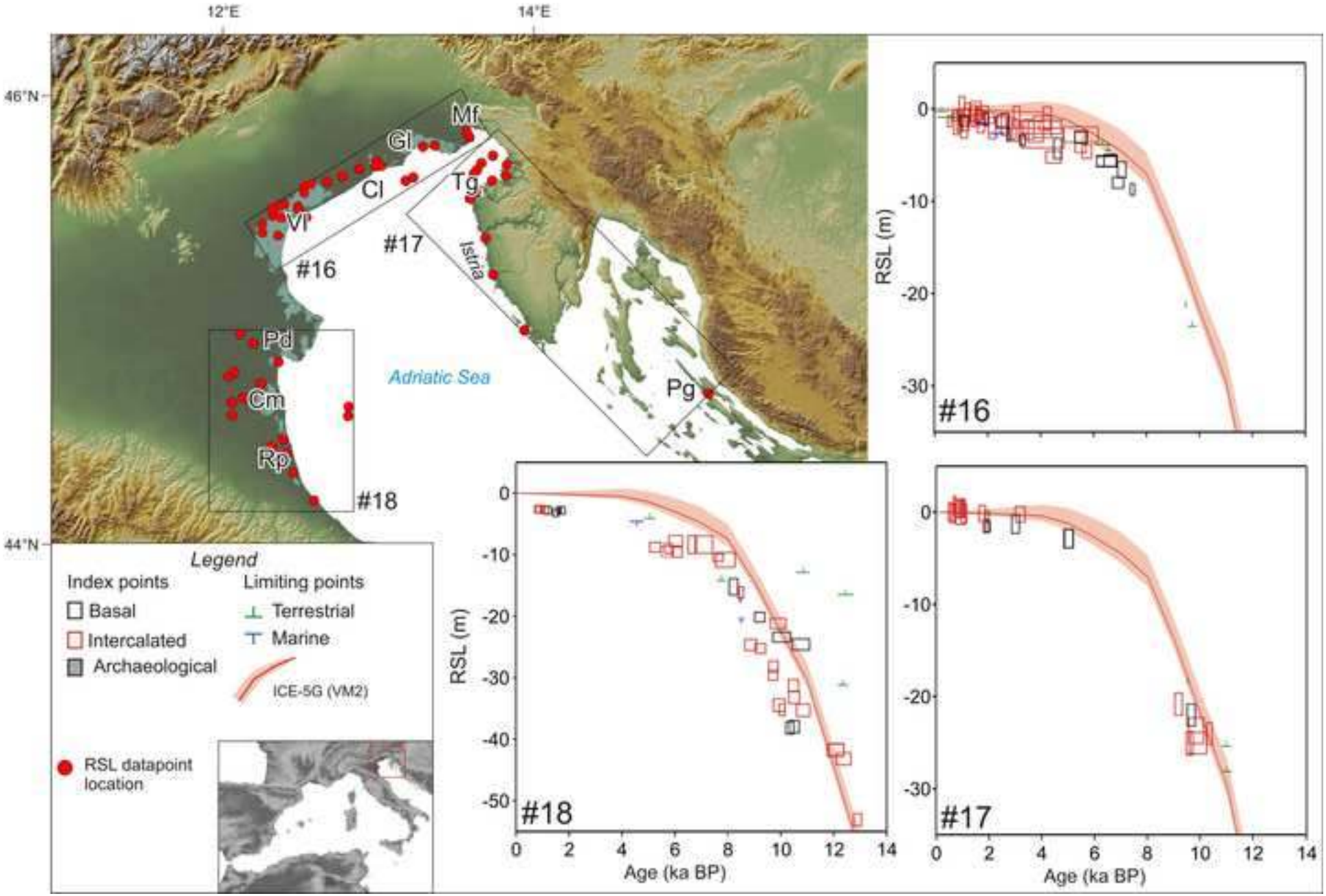

Figure 11

Click here to download high resolution image

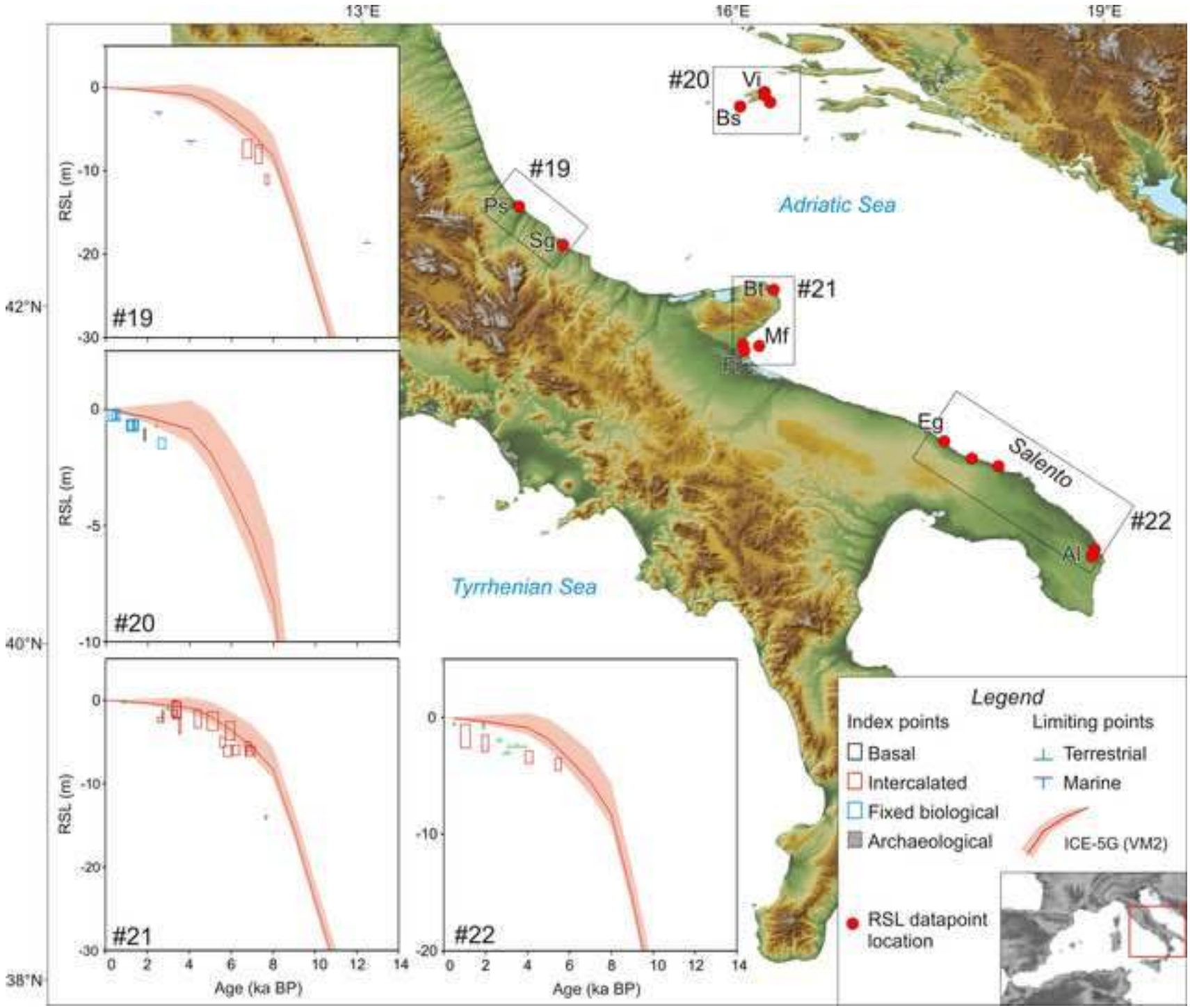

Figure 12

Click here to download high resolution image

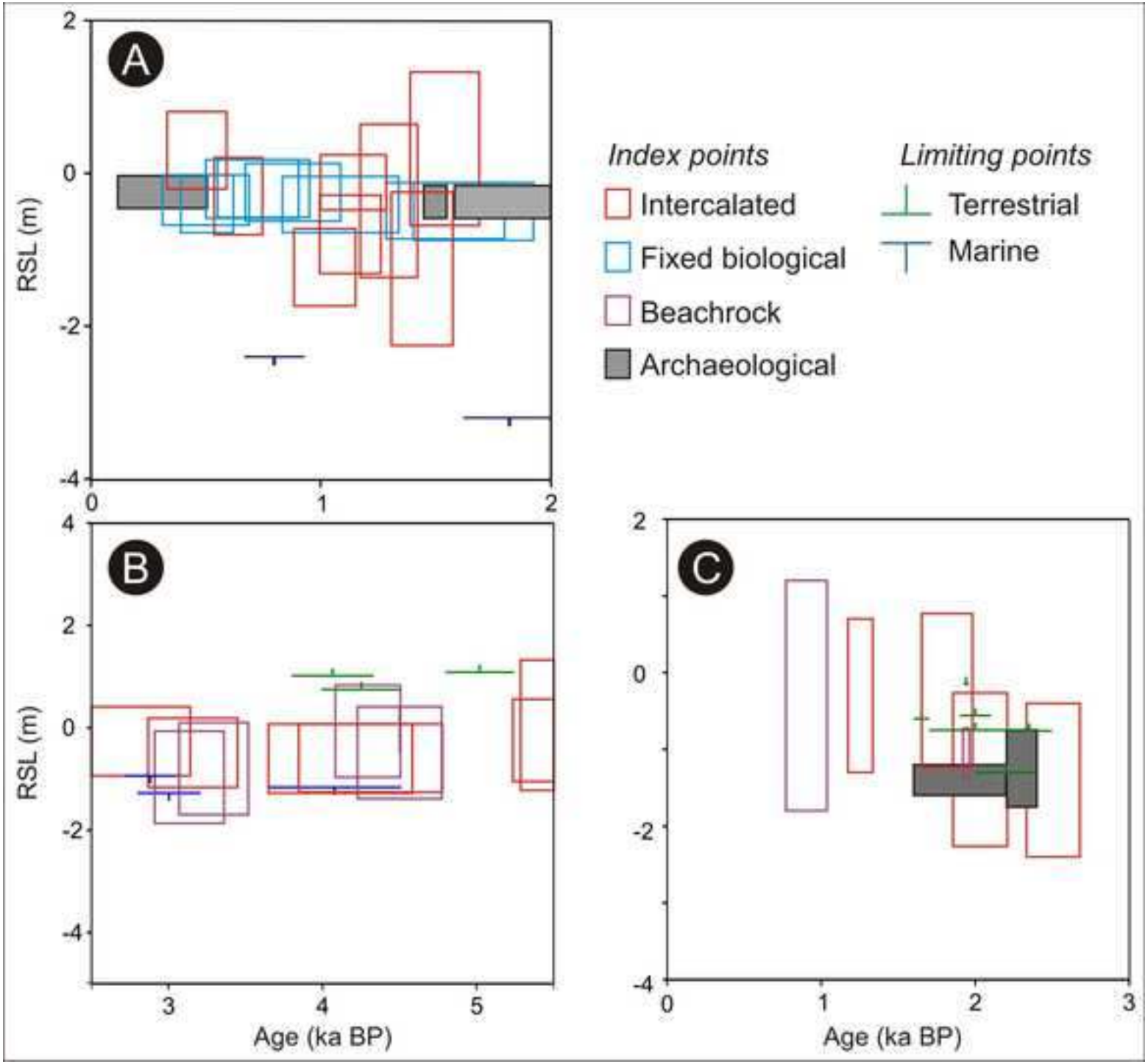

Figure 13

Click here to download high resolution image